CATHODIC PROTECTION FOR ON- AND OFF-SHORE STRUCTURES

By

CHAO LIU

A THESIS PRESENTED TO THE GRADUATE SCHOOL
OF THE UNIVERSITY OF FLORIDA IN PARTIAL FULFILLMENT
OF THE REQUIREMENTS FOR THE DEGREE OF
MASTER OF SCIENCE

UNIVERSITY OF FLORIDA

2012

To my parents and my grandparents

ACKNOWLEDGMENTS

Here I would like to thank my advisor, Professor Mark E. Orazem, for his teaching and guidance. I thank Professor Jennifer Sinclair Curtis for her support as well. I also want to thank every colleague in my group: Alok Shankar, Rui Kong, Ya-Chiao Chang, Christopher Cleveland, Salim Erol, Yan Yu, Yu-min Chen, Darshit Shah and Pei-han Chiu.

TABLE OF CONTENTS

page

LIST OF TABLES

LIST OF FIGURES

LIST OF ABBREVIATIONS

BEM	Boundary Element Method
CP	Cathodic protection
CP3D	Three dimensional cathodic protection simulation system
CSE	Copper Sulfate Electrode
FEM	Finite Element Method
ICCP	Impressed current cathodic protection

Abstract of Thesis Presented to the Graduate School
of the University of Florida in Partial Fulfillment of the
Requirements for the Degree of Master of Science

CATHODIC PROTECTION FOR ON- AND OFF-SHORE STRUCTURES

By

Chao Liu

May 2012

Chair: Mark E. Orazem
Major: Chemical Engineering

Natural gas and liquid petroleum products have been transported by an extensive network of steel pipelines all over the world. Steel pipelines are usually buried in soil or aquatic environment where electrolyte contains oxygen, and then they are subject to corrosion.

Corrosion even can happen under cathodic protection. One type of this corrosion is caused by stray current effect. Stray currents from the anodic part of the cathodic protection system are picked by a foreign pipe and result in localized corrosion at the site where stray current leaves from the foreign pipe. Thus, it is very important to optimize the design of cathodic protection system and design the methods to prevent the pipelines from corrosion caused by stray currents.

In the thesis, a CP3D numerical simulation model was used to simulate the stray current effects that happened in a cathodic protection system, understand the interaction behavior between the protected pipe and the unprotected pipe in the system, and predict the position on the unprotected pipe where localized corrosion occurred. Methods of modeling stray current effects were then applied to simulate rectifier war in soil and seawater environment respectively. The mechanism that underlies rectifier

wars, in which interference of cathodic protection systems results in under-protection, was clearly illustrated. In addition, simulations were used to calculate the minimum number of anodes needed to provide adequate cathodic protection in both soil and seawater environments.

CHAPTER 1
INTRODUCTION

With the development of modern industries from the beginning of the twentieth century, increasing amounts of petroleum products and natural gas have been transported by long steel pipelines. The steel pipelines are usually buried in soil environments (on-shore environment) or aquatic environment (off-shore environment). As these environments contain oxygen, the steel pipelines and their surroundings constitute an electrochemical system where corrosion happens. Corrosion is one of main causes of pipeline failures.

It was estimated that the average annual cost of corrosion of infrastructure is $22.6 billion from 1997 to 1999 in U.S [1]. The annual cost of gas and liquid transmission pipelines corrosion is nearly $7.0 billion, as is shown in Figure 1-1. It is therefore essential to apply cathodic protection to the buried pipelines and prevent them from corrosion. However, even if cathodic protection is applied, severe pipeline accidents may happen due to inadequate cathodic protection.

For example, in 1996, a pipeline transporting fuel oil ruptured where the ruptured section of the pipeline crossed a river in South Carolina [2]. 957,600 gallons of fuel oil came out of the ruptured pipeline and flowed into the river. This accident killed nearly 35,000 fish and resulted in an economic loss more than $20.5 million. The subsequent investigation after the accident indicated that the corrosion problem had already happened before the accident, and that the river current had washed away the coating of the ruptured section. This accident was attributed to the pipeline controller’s negligence and inadequate cathodic protection.

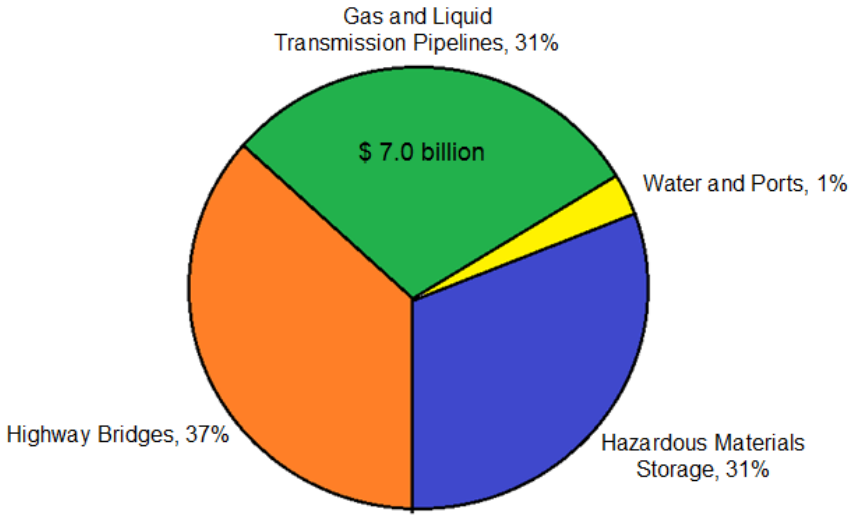

Figure 1-1. Annual cost of corrosion of gas and liquid transmission pipelines

CHAPTER 2
LITERATURE REVIEW

Cathodic Protection and Stray Current Effects

It is essential to understand the corrosion behavior in a cathodic protection system and to take corresponding measures to prevent corrosion of the pipelines. The first step is to know what cathodic protection is. Cathodic protection is a method in which the corrosion of a metal surface is controlled by letting it be the cathode of an electrochemical cell. An anode that is connected to the pipeline is applied to provide external current as is shown in Figure 2-1. There are mainly two ways to apply cathodic protection to a steel pipeline [3]: 1) by applying an external power supply (Impressed current cathodic protection: ICCP), or 2) by placing it in contact with a more electrochemically active metal to form a galvanic couple. In the first method, a rectifier is usually used to provide power supply. In the second method, the anode is called a sacrificial anode or galvanic anode since it is consumed during the cathodic protection.

The second step is to understand a typical corrosion behavior in cathodic protection systems associated with stray current effects. Stray currents may accompany with impressed current cathodic protection systems in the manner shown in Figure 2-2. In Figure 2-2, a foreign steel pipe is introduced close to the cathodic protection system. Stray currents from the anode of the cathodic protection system can flow into a foreign pipe. The site of the foreign pipe where stray currents leave will experience localized corrosion. The solution to prevent stray current effects is to use electrical bonding to connect the pipe and the tank as is shown in Figure 2-3.

Electrochemical Kinetics

In order to develop a mathematical model describing cathodic protection of the steel pipelines, it is essential to know the boundary conditions at the pipe steel and anode surface where electrochemical reactions are involved. Here the Butler-Volmer equation is applied, which is one of the most fundamental relationships in electrochemical kinetics. It demonstrates how the electrode current depends on the electrode potential [4].

Bockris and other researchers indicated that the rate of dissolution and deposition of Iron depends on pH value [5]. There are several mechanisms discussed by Bockris [5]. Since buried structures under cathodic protection are in soil form alkaline environments [6], the mechanism for the dissolution of iron in this case can be written as

$$Fe^{2+} + 2OH^- \xrightarrow{\text{R.D.S.}} Fe(OH)_2 + 2e^- \tag{2-1}$$

Here R.D.S. means rate-determining step. This reaction is followed by

$$Fe(OH)_2 \rightleftarrows Fe^{2+} + 2OH^- \tag{2-2}$$

By combining equation (2-1) and (2-2), the net equation (2-3) can be obtained as

$$Fe \rightleftarrows Fe^{2+} + 2e^- \tag{2-3}$$

The deposition of iron from ferrous hydroxide can be represented as

$$Fe(OH)_2 \rightleftarrows Fe^{2+} + 2OH^- \tag{2-4}$$

or, after introduction of equation (2-3), as

$$Fe(OH)_2 + 2e^- \xrightarrow{\text{R.D.S}} Fe + 2OH^- \tag{2-5}$$

Bockris and other researchers also described the anodic current density in terms of hydroxide ion activity and electrochemical potential as [5]

$$i_a = k_{a,Fe} a_{OH^-} e^{[\frac{(1-\beta)VF}{RT}]} \quad (2\text{-}6)$$

where $k_{a,Fe}$ is the kinetic rate constant, a_{OH^-} is the activity of OH^- ions, β is the transfer coefficient, V is potential difference between metal and solution (Φ_{metal}-$\Phi_{solution}$), F is Faraday's constant, R is the Gas Constant and T is the temperature of the electrochemical system. Here, the activity of ions and pH are in a linear relationship. The expression of cathodic current can be written as

$$i_c = k_{c,Fe} a_{Fe^{2+}} a_{OH^-} e^{[\frac{-\beta VF}{RT}]} \quad (2\text{-}7)$$

where $a_{Fe^{2+}}$ is the activity of Fe^{2+} ions. The net current density i_{total} can be expressed as [4]

$$i_{total} = i_a - i_c \quad (2\text{-}8)$$

The equilibrium potential V_0 can be obtained by setting equation (2-8) equal to zero and solving for V

$$V_0 = \frac{RT}{F} \ln[\frac{\kappa_{c,Fe} a_{Fe^{2+}}}{\kappa_{a,Fe}}] \quad (2\text{-}9)$$

The exchange current density can be obtained by putting equation (2-9) into equation (2-6) and solving for i_a

$$i_0 = \kappa_{a,Fe} a_{OH^-} e^{[\frac{(1-\beta)V_0F}{RT}]} \quad (2\text{-}10)$$

Putting equation (2-9) into equation (2-10) yields

$$i_0 = \kappa_{a,Fe}^{\beta} \kappa_{c,Fe}^{1-\beta} a_{Fe^{2+}}^{1-\beta} a_{OH^-} \quad (2\text{-}11)$$

Equation (2-8) can be rewritten in terms of the exchange current density as

$$i_{Fe}=10^{(\frac{V-E_a}{\beta_a})}-10^{(\frac{V-Ec}{\beta_c})} \quad (2\text{-}12)$$

where β_a and β_c are Tafel slopes

$$\beta_a=\frac{2.303RT}{(1-\beta)F} \quad (2\text{-}13)$$

$$\beta_c=\frac{2.303RT}{-\beta F} \quad (2\text{-}14)$$

and E_c and E_a are standard potentials for anodic and cathodic reactions respectively.

In a practical corrosion system, such as corrosion of steel pipelines, the anodic reaction is

$$Fe \rightarrow Fe^{2+}+2e^- \quad (2\text{-}15)$$

This is often accompanied by two cathodic reactions: one is called the oxygen reduction reaction

$$O_2+2H_2O+4e^- \longrightarrow 4OH^- \quad (2\text{-}16)$$

The other possible cathodic protection is called the hydrogen evolution reaction

$$2H_2O+2e^- \longrightarrow H_2+2OH^- \quad (2\text{-}17)$$

The potential required for oxygen reduction reaction is more positive than that for hydrogen evolution reaction. There are many papers which illustrate the mechanism of the hydrogen evolution reaction (HER) [7-11]. The hydrogen evolution current density can be written as

$$i_{H_2}=10^{\left[\frac{V-E_{a,H_2}}{\beta_{a,H_2}}\right]}-10^{\left[\frac{V-E_{c,H_2}}{\beta_{c,H_2}}\right]} \quad (2\text{-}18)$$

Thus, the total current can be expressed as the sum of net current density with respect to dissolution of metal, oxygen reduction reaction and hydrogen which is shown in equation (2-19)

$$i=10^{\left[\frac{V-E_{a,Fe}}{\beta_{a,Fe}}\right]}-10^{\left[\frac{V-E_{c,Fe}}{\beta_{c,Fe}}\right]}+10^{\left[\frac{V-E_{a,O_2}}{\beta_{a,O_2}}\right]}-10^{\left[\frac{V-E_{c,O_2}}{\beta_{c,O_2}}\right]}+10^{\left[\frac{V-E_{a,H_2}}{\beta_{a,H_2}}\right]}-10^{\left[\frac{V-E_{c,H_2}}{\beta_{c,H_2}}\right]} \quad (2\text{-}19)$$

The corrosion potential V_{Corr} is the potential difference between a freely corroding surface and a reference electrode. We can obtain the corrosion potential V_{Corr} by setting equation (2-19) equal to zero. It should be noticed that V_{Corr} is different from equilibrium potential which is shown in equation (2-9) since there is more than one reaction which occurs in a freely corroding system [12].

Bare Steel Pipeline

If a numerical method is used to build a corrosion model, equation (2-19) can be applied to describe the kinetics at the boundary. In order to simplify equation (2-19), some terms which are out of potential range of interest can be cancelled out. If a mass-transfer limitation factor is considered, the total current density will be written as

$$i_{total}=10^{\frac{V-\Phi-E_{Fe}}{\beta_{Fe}}}-\left(\frac{1}{i_{lim,O_2}}-10^{\frac{V-\Phi-E_{O_2}}{\beta_{O_2}}}\right)^{-1}-10^{\frac{-(V-\Phi-E_{H_2})}{\beta_{H_2}}} \quad (2\text{-}20)$$

where i_{lim,O_2} is the mass transfer limited current density for oxygen reduction, $V-\Phi$ is the potential difference between metal and solution. Nisoncioglu was the first to consider mass transfer limitation into this expression of total current density [13-15]. Yan and other researchers also used this total current density expression in a numerical

simulation to determine potential and current density distribution along a cathodically protected pipeline in artificial seawater numerically [16].

Equation (2-20) was also applied to describe corrosion of bare steel in steady state soil condition [17]. It is noticed that there is no mass transfer limitation term for hydrogen evolution reaction in equation (2-20) because it was assumed that adequate water exit in the vicinity of steel pipe to maintain hydrogen evolution reaction [12].

Pipeline with Coatings

Coatings are needed to be applied to the metal surface. There are three common types of coatings: organic barrier coatings, chemically active coatings and sacrificial metallic coatings [18]. Of these three types of coatings, organic barrier coatings, especially polymers are usually used.

A coating is considered to be barrier of ions and oxygen transportation. If diffusion barrier effect of the coatings is considered, the equation (2-20) will be modified as:

$$i_{total} = \frac{A_{pore}}{A}\left[10^{\frac{V-\Phi_{in}-E_{Fe}}{\beta_{Fe}}} - \left(\frac{1}{(1-\alpha_{block})i_{lim,O_2}} - 10^{\frac{V-\Phi_{in}-E_{O_2}}{\beta_{O_2}}}\right)^{-1} - 10^{\frac{-(V-\Phi_{in}-E_{H_2})}{\beta_{H_2}}}\right] \quad (2\text{-}21)$$

where $\frac{A_{pore}}{A}$ is the effective surface area available for reactions, Φ_{in} is the potential at the underside of the coating just above the steel and α_{block} is the reduction to the transport of oxygen through the barrier [12]. This form was published by Riemer and Orazem [19-20].

Orazem and Kenelley expressed the potential drop through the coating as

$$i_{total} = \frac{\Phi - \Phi_{in}}{\rho\delta} \quad (2\text{-}22)$$

where Φ is the potential in the electrolyte next to the coating, ρ is the resistivity of the coating and δ is the thickness of the coating. Substitute equation (2-22) into equation (2-21)

$$\frac{A(\Phi - \Phi_{in})}{A_{pore}\rho\delta} = \left[10^{\frac{V-\Phi_{in}-E_{Fe}}{\beta_{Fe}}} - \left(\frac{1}{(1-\alpha_{block})i_{lim,O_2}} - 10^{\frac{V-\Phi_{in}-E_{O_2}}{\beta_{O_2}}} \right)^{-1} - 10^{\frac{-(V-\Phi_{in}-E_{H_2})}{\beta_{H_2}}} \right] \quad (2\text{-}23)$$

Φ_{in} can be obtained by applying the Newton Ralphson method. If Φ_{in} is calculated, the current density can be obtained by using equation (2-22).

Cathodic Protection Methods

Anodes experience the similar electrochemical process as the steel pipelines do. In cathodic protection, both galvanic anodes and impressed current anodes can be applied.

Galvanic Anodes (Sacrificial Anodes)

Galvanic anodes are more electrochemically active than the metal pipeline. The electrical driving force varies with materials of the anodes, so it is very important to choose the proper anode in different environments. In soil environment, in which larger driving force is required, zinc and magnesium are used. In seawater environment, in which smaller driving force is needed, aluminum is used [18].

Riemer [12] introduced a model for current density in a galvanic anode

$$i_{\text{galvanic anode}} = i_{O_2}\left(10^{\frac{V-\Phi-E_{corr}}{\beta_{anode}}} - 1\right) \quad (2\text{-}24)$$

where i_{O_2} is the mass transfer limited current density with respect to reduction of oxygen. Φ is the potential in the electrolyte next to the anode surface, E_{Corr} is the equilibrium

corrosion potential, and β_{anode} is the Tafel slope for the anodic reaction. Table 2-1 gives some parameters for different types of galvanic anodes.

Impressed Current Anodes

Impressed current systems depend on an external power source to provide current. A direct-current (DC) rectifier is usually used. The negative terminal of the rectifier is connected to the steel pipeline, and the positive terminal of the rectifier is connected to a dimensionally stable anode [12]. The rectifier provides a larger potential difference (electrical driving force) than provided by sacrificial anodes. Thus, impressed current cathodic protection systems use fewer anodes than galvanic cathodic protection systems when protecting the same section of the pipe. Since dimensionally stable anodes are applied in impressed current cathodic protection systems, the anodic reaction cannot be dissolution of metal, the most possible anodic reactions will be

$$2H_2O \longrightarrow O_2 + 4H^+ + 4e^- \tag{2-25}$$

and

$$2Cl^- \longrightarrow Cl_2 + 2e^- \tag{2-26}$$

In impressed current anode system, the potential that supplied by the rectifier is considered, so equation (2-24) is modified to be

$$i_{\text{impressed current anode}} = i_{O_2}\left(10^{\frac{V-\Phi-\Delta V_{\text{rectifier}}-E_{O_2}}{\beta_{O_2}}} - 1\right) \tag{2-27}$$

where $\Delta V_{\text{rectifier}}$ is the voltage added by the rectifier, V is the potential of the anode, Φ is the potential in the electrolyte just next to the surface of the anode, E_{O_2} is the equilibrium potential for evolution of oxygen, and β_{O_2} is the Tafel slope for the oxygen evolution

reaction. If the system is in a chloride ion dominant environment, equation (2-27) will be written as

$$i_{\text{impressed current anode}} = i_{O_2}\left(10^{\frac{V\text{-}\Phi\text{-}\Delta V_{\text{rectifier}}\text{-}E_{Cl_2}}{\beta_{Cl_2}}}\text{-}1\right) \qquad \text{(2-28)}$$

where E_{Cl_2} is the equilibrium potential for evolution of chloride and β_{Cl_2} is the Tafel slope for the chloride evolution reaction.

Table 2-1. Parameters for some typical galvanic anodes

Anode type	E_{eql} (mV CSE)	β (mV/ decade)	i_{O2} (μA/cm^2)
Al	-1.0	60	1.0
Zn	-1.1	60	1.0
Mg(Standard)	-1.5	60	1.0
Mg(High potential)	-1.75	60	1.0

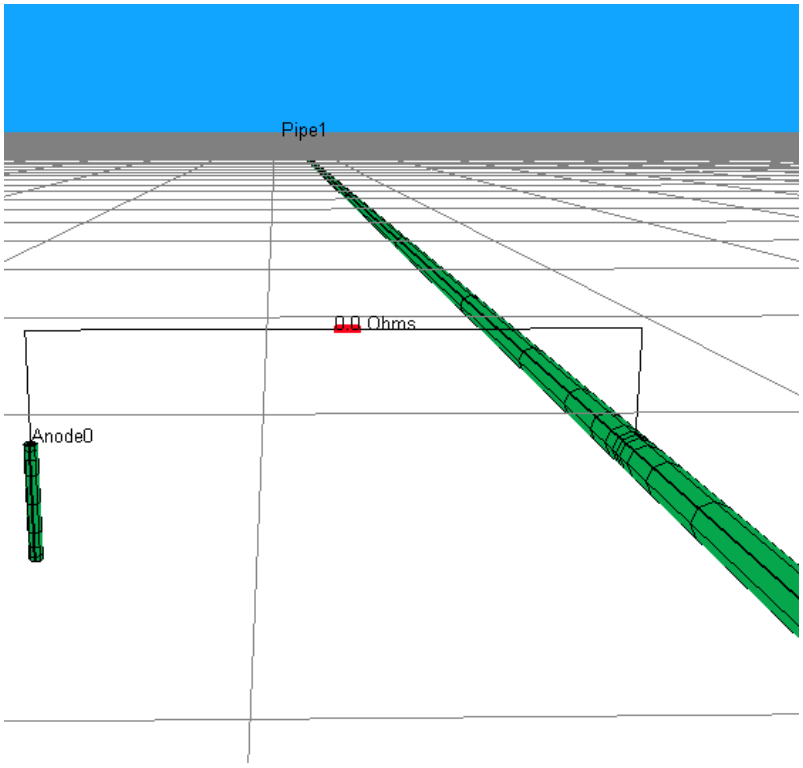

Figure 2-1. Cathodic protection system of buried steel pipeline. The shorter vertical rod represents anode, the longer horizontal rod represents pipeline.

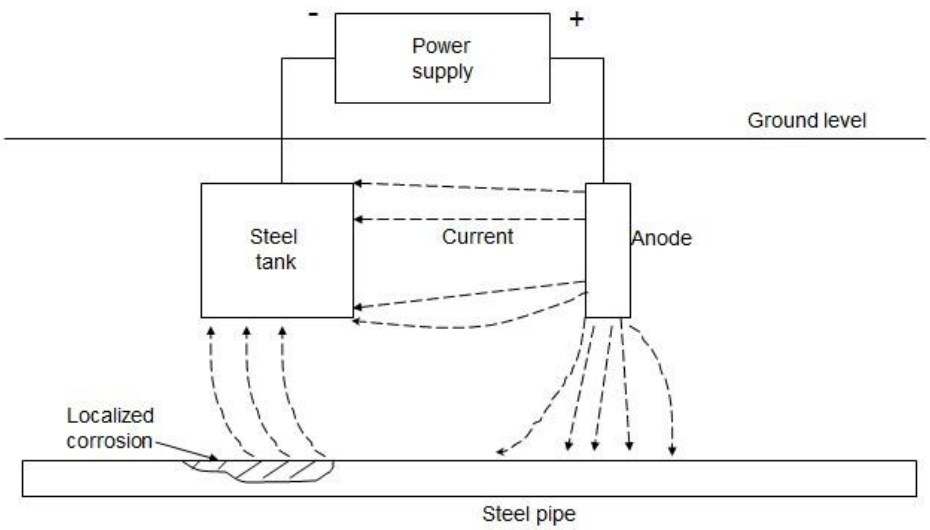

Figure 2-2. Stray current resulting from cathodic protection

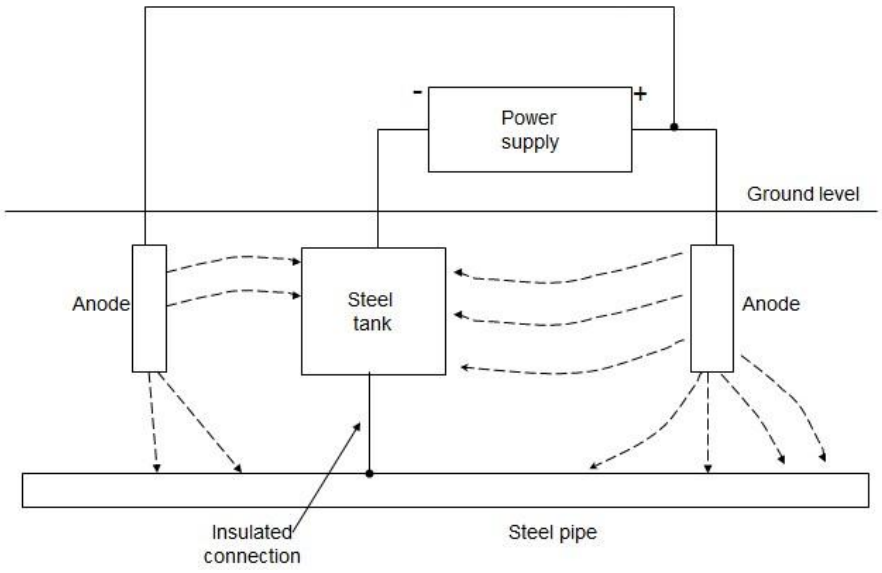

Figure 2-3. Prevention of stray current corrosion by proper design

CHAPTER 3
MATHEMATICAL MODEL OF CATHODIC PPOTECTION

Domains for the Flow of Current

In practical cathodic protection for pipelines, the potential and current density vary along the metal structures and the electrolyte adjacent to their surface. The current density and potential distributions in the soil and along the pipe influence cathodic protection. Hence, there are two different domains for flow of current: the soil domain and the internal domain [12].

Soil Domain

The boundary of the soil domain is along with the surfaces of the steel pipeline and anodes. As is discussed in Chapter 2, expressions for current density depend on the pipe surface property and on the materials of anodes, in other words, the boundary conditions for the soil domain vary with the kinetics involved.

The Laplace's equation governs the soil domain. Newman gives a detailed derivation for governing Laplace's equation [21]. The flux density of each dissolved species in a dilute electrolytic solution is written as

$$\underset{\text{flux}}{N_i} = \underbrace{-z_i u_i F c_i \nabla\Phi}_{\text{migration}} \underbrace{- D_i \nabla c_i}_{\text{diffusion}} + \underbrace{c_i v}_{\text{convection}} \tag{3-1}$$

where N_i is the flux density of species i, z_i is the charge number of species i, u_i is the mobility of species i, F is the Faraday Constant, c_i is the concentration of species i, $\nabla\Phi$ is the electric field, D_i is the diffusion coefficient of species i, ∇c_i is the concentration gradient of species i, and v is the fluid velocity. Here N_i, $\nabla\Phi$, ∇c_i and v are vectors. Equation (3-1) applies for dilute electrolytes.

The current density can be expressed in terms of flux as

$$i = \mathrm{F}\sum_{\mathrm{i}} z_{\mathrm{i}} N_{\mathrm{i}} \tag{3-2}$$

Substitution of equation (3-2) into equation (3-1) yields

$$i = -\mathrm{F}^2 \nabla\Phi \sum_{\mathrm{i}} z_{\mathrm{i}}^2 u_{\mathrm{i}} c_{\mathrm{i}} - \mathrm{F}\sum_{\mathrm{i}} z_{\mathrm{i}} D_{\mathrm{i}} \nabla c_{\mathrm{i}} + \mathrm{F}v\sum_{\mathrm{i}} z_{\mathrm{i}} c_{\mathrm{i}} \tag{3-3}$$

The last term can be cancelled out in the equation because of electroneutrality. The assumption that there are no concentration variations in the solution is made, so the second term of equation (3-3) is equal to zero. Finally, equation (3-3) reduces to

$$i = -\kappa\nabla\Phi \tag{3-4}$$

where

$$\kappa = \mathrm{F}^2 \sum_{\mathrm{i}} z_{\mathrm{i}}^2 u_{\mathrm{i}} c_{\mathrm{i}} \tag{3-5}$$

Equation (3-4) is an expression of Ohm's law. It applies when there are no graduate concentration gradients in electrolytes.

The expression of conservation of charge gives

$$\nabla \cdot i = 0 \tag{3-6}$$

Substitution of equation (3-4) into equation (3-6) yields

$$\nabla^2 \Phi = 0 \tag{3-7}$$

which is known as Laplace's equation

Internal Domain

The internal domain contains the internal pipe metal, the anode metal and the connecting wire between anodes and pipelines [12]. The current flow in the internal domain is governed by the three-dimensional Laplace's equation [12], i.e.,

$$\nabla \cdot (\kappa \nabla V) = 0 \tag{3-8}$$

where V is the potential difference between the potential of the metal and reference value and κ is the material conductivity. The conductivity κ is not always a constant. In some situations, the potential drop in internal domain can be expressed as [12], i.e.,

$$\Delta V = IR = I\rho\frac{L}{A} \tag{3-9}$$

where R is the wire resistance, ρ is the electrical resistivity, L is the length of wire, and A is the cross sectional area.

Numerical Methods for Solving Laplace's Equation

Two numerical methods were used in solving the Laplace's equation: boundary element method and finite element method. The boundary element method is used to solve for soil domain with nonlinear boundary condition. Brebbia was the first to use weighted residual techniques to solve for potential with the boundary element method. [22]. Aoki simplified the corrosion behavior in the Laplace's equation with simple, nonlinear boundary conditions and solved it by using the boundary element method [23]. Aoki also estimated the optimum impressed-current-anode locations and optimum current output from the anode by applying the boundary element method [24].

The finite element method is used in internal domain. This idea was first brought by Brichau and other researchers [25]. They linked the finite element method with the developed boundary element method solution in soil environments to illustrate cathodic protection numerically. FEM/BEM coupling approach is applied at the interface between soil domain and internal domain [12].

Boundary Element Method

A symmetric Galerkin Boundary Element Method [26] is applied to the constant boundary condition since the direct Boundary Element Method will create non-symmetric matrices, and fast iterative methods cannot be employed to solve the resulting linear PDE equation $Ax = b$.

The boundary element formulations in this method [12] can be written as

$$\int_{\Gamma} \phi_i \Phi_i d\Gamma_i + \int_{\Gamma} \phi_i \int_{\Gamma} \Phi(\vec{n} \cdot \nabla G_{i,j}) d\Gamma_j d\Gamma_i = \int_{\Gamma} \phi_i \int_{\Gamma} G_{i,j} (\vec{n} \cdot \nabla \Phi) d\Gamma_j d\Gamma_i \tag{3-10}$$

and

$$\int_{\Gamma} \phi_i \kappa(\vec{n}_i \cdot \nabla \Phi_i) d\Gamma_i + \int_{\Gamma} \phi_i \int_{\Gamma} \Phi \kappa(\vec{n}_i \cdot \nabla(\vec{n}_j \cdot \nabla G_{i,j})) d\Gamma_j d\Gamma_i = \int_{\Gamma} \phi_i \int_{\Gamma} (\vec{n}_i \cdot \nabla G_{i,j}) \kappa(\vec{n}_j \cdot \nabla \Phi) d\Gamma_j d\Gamma_i \tag{3-11}$$

where i and j represent the i's and j's source element respectively, Γ is the boundary of the domain, ϕ is the shape function, κ is a constant, $\vec{n}$ is the outward normal vector to the surface of the domain, Φ is the potential of electrolyte, Γ is the boundary of the domain, and G is the Green function.

However, the symmetric Galerkin Boundary Element Method does not work for nonlinear boundary conditions, so the direct Boundary Element Method is applied to a surface that can be divided into individual finite elements. The form of this method can be written as

$$c_i \Phi_i + \int_{\Gamma} \Phi(\vec{n} \cdot \nabla G_{i,j}) d\Gamma = \int_{\Gamma} G_{i,j} (\vec{n} \cdot \nabla \Phi) d\Gamma \tag{3-12}$$

More detail is provided by Riemer [12].

Finite Element Method

The formula used in this type of Finite Element Method [12] is

$$\sum_i \left[h \iint_{\Omega^{(e)}} \sum_k \frac{\partial \phi_i}{\partial x_k} \kappa \cdot \frac{\partial \phi_i}{\partial x_k} \sqrt{|J|} d\xi d\eta \right] = - \oiint_{\Gamma_{(e)}} w \kappa (\vec{n} \cdot \nabla V) ds \tag{3-13}$$

where i is the $i's$ element, h is the thickness of the steel, $\Omega^{(e)}$ is the domain of parent elements, ϕ is the shape function, κ is a constant, J is the Jacobian. $d\xi d\eta$ is the shell element, w is the weighing function, $\vec{n}$ is the outward normal vector to the surface of the domain, and V is the potential of metal.

Coupling FEM/BEM

The formula applicable at the interface between the soil domain and internal domain [12] is written as

$$\sum_i \left[h \iint_{\Omega^{(e)}} \sum_k \frac{\partial \phi_i}{\partial x_k} \kappa \cdot \frac{\partial \phi_i}{\partial x_k} \sqrt{|J|} d\xi d\eta \right] = - \oiint_{\Gamma_{(e)}} w \kappa_{\text{soil}} (\vec{n} \cdot \nabla \Phi) ds \tag{3-14}$$

where these parameters are described in the above two sections. More detail is provided by Riemer [12].

CHAPTER 4
RESULTS AND ANALYSIS

Dimensional Analysis for Primary Current Distribution

The Buckingham method was used in dimensional analysis [27]. It is a method of obtaining the important dimensionless numbers constructed by the original variables. This method states that if a certain number, n, of physical variables are involved in an equation, and the units of these physical variables are given in terms of m fundamental units, then the equation can be expressed in terms of $(n-m)$ independent dimensionless variables.

It is essential to understand the variables which affect the current density distribution along a single pipe. There are nine variables involved in the current distribution which are shown in the Table 4-1. By applying the Buckingham method, the relationship between these nine variables can be written as

$$\frac{LR}{\rho} = \mathrm{f}\left(\frac{d}{L}, \frac{D_{\mathrm{L}}}{L}, \frac{H_{\mathrm{L}}}{L}, \frac{D_{\mathrm{a}}}{L}, \frac{L_{\mathrm{a}}}{L}, \frac{H_{\mathrm{a}}}{L}\right) \tag{4-1}$$

where $\frac{LR}{\rho}$ is the normalized resistance, $\frac{d}{L}$ is the normalized anode distance, $\frac{D_{\mathrm{L}}}{L}$ is the normalized diameter of the pipe, $\frac{H_{\mathrm{L}}}{L}$ is the normalized depth of the pipe, $\frac{D_{\mathrm{a}}}{L}$ is the normalized diameter of the anode, $\frac{L_{\mathrm{a}}}{L}$ is the normalized length of the anode, and $\frac{H_{\mathrm{a}}}{L}$ is the normalized depth of the anode. The normalized resistance is a function of the other six normalized numbers.

For a primary current distribution, the kinetic resistance is neglected since the ohmic resistance dominates. Thus the resistance R can be expressed in terms of Ohm's Law as

$$R = \frac{V}{I} \tag{4-2}$$

Equation (4-1) may then be modified as

$$\frac{LV}{\rho I} = \mathrm{f}\left(\frac{d}{L}, \frac{D_{\mathrm{L}}}{L}, \frac{H_{\mathrm{L}}}{L}, \frac{D_{\mathrm{a}}}{L}, \frac{L_{\mathrm{a}}}{L}, \frac{H_{\mathrm{a}}}{L}\right) \tag{4-3}$$

Among these variables, D_{L} and H_{L} do not have a significant impact on the resistance; whereas, L_{a}, D_{a}, H_{a} and d are dominant variables. D_{L} and H_{L} can be proved to be insignificant by running the CP3D simulation. By altering the value of D_{L} or H_{L}, and keeping the rest of the variables fixed, it can be observed that the current I does not change significantly.

In order to get the relationship between the normalized resistance and the dimensionless number related to the anode properties, the first step was to specify D_{L} and H_{L}, which were specified to be 0.1m and 1m respectively, so the normalized resistance was controlled by the other four dimensionless variables. The length of pipe was chosen to be 6000m and the soil resistivity was chosen to be 10,000 ohm-cm. The second step was to scale the normalized resistance. A proper method was to divide it by another normalized resistance which is obtained by Dwight's formula. Dwight's formula was used to calculate the resistance of a vertical rod. It is written as

$$R = \left(\frac{0.005\rho}{\pi L}\right) \times \left(\ln\frac{8L}{d} - 1\right) \tag{4-4}$$

where ρ is the soil resistivity, L is the length of an anode, and d is the diameter of the anode. Under the condition specified above, the resistance calculated by Dwight's formula is

$$R_{\text{Dwight}}=(\frac{0.005\times10000}{\pi\times1})(\ln\frac{8\times1}{0.1}\text{-}1)=53.82\text{ohm} \tag{4-5}$$

The corresponding normalized resistance can be written as

$$\frac{LR_{\text{Dwight}}}{\rho}=\frac{6000\text{m}\times53.82\text{ohm}}{100\text{ohm-m}}=3229.2 \tag{4-6}$$

Thus, a scaled resistance R_{scale} can be defined as

$$R_{\text{scale}}=\frac{\frac{LR}{\rho}}{\frac{LR_{\text{Dwight}}}{\rho}}=\frac{R}{R_{\text{Dwight}}} \tag{4-7}$$

From the previous analysis, d, L_a, D_a, and H_a are dominant variables and their effects on the current density distribution along the single pipe can be obtained from the relationships between normalized resistance and the four normalized dominant variables respectively. The simulation used the base condition of L=6000m, D_L =0.3m, d=10m, D_a = 0.1m, L_a = 1m, H_a = 1m, the pipe with equal potential of 1V. The potential difference between pipe and anode is always equal to 1V. The process of modeling was: 1) Increase $\frac{d}{L}$, keeping $\frac{H_a}{L}$, $\frac{D_a}{L}$ and $\frac{L_a}{L}$ fixed (Figure 4-1). 2) Increase $\frac{H_a}{L}$, keeping $\frac{d}{L}$, $\frac{D_a}{L}$ and $\frac{L_a}{L}$ fixed (Figure 4-2). 3) Increase $\frac{D_a}{L}$, keeping $\frac{H_a}{L}$, $\frac{d}{L}$ and $\frac{L_a}{L}$ fixed (Figure 4-3). 4) Increase $\frac{L_a}{L}$, keeping $\frac{H_a}{L}$, $\frac{d}{L}$ and $\frac{D_a}{L}$ fixed (Figure 4-4). From these four

relationships, it was concluded that: 1) normalized resistance increases with the anode distance initially and then remains stable. The probable explanation is that more ohmic resistance is added between anode the pipe if the anode distance increases. 2) Normalized resistance deceases sharply as the depth of anode goes up and then remains stable. If the depth of anode is increased, more current will come out of the top of the anode and go to the pipe, and the corresponding normalized resistance will decrease. 3) The normalized resistance deceases when normalized diameter of anode increases. The reason is that the dimension of the anode will expand with increasing diameter of the anode. 4) The normalized resistance decreases as normalized length of anode increases. The explanation is the same with observation 3).

In addition to obtaining the relationship between normalized resistance and anode variables, the relationship between scaled resistance (normalized resistance divided by Dwight formula) and the anode variables was also needed since it is essential to compare the simulation results with analytical solution. The four relationships are shown from Figure 4-5 to Figure 4-8. The corresponding conclusions can be obtained: 1) The calculate resistance is closer to that provided by the Dwight formula at a larger anode distances. 2) The calculated resistance is closer to that provided by the Dwight Formula at smaller depth of anode. 3) The calculated resistance is closer to the that provided by the Dwight Formula at smaller and larger diameters of anode respectively. 4) The calculate resistance is closer that provided by the Dwight Formula at a larger lengths of anode. Particularly, the scaled resistance increases with normalized length of anode under the condition of 0m < D_a <0.8m, while it decreases initially and then increases under the condition of D_a ≥0.8m.

The base condition was changed to different sets of new conditions such that the relationships between resistance and one anode variable were obtained under different sets of another anode variable, keeping the remaining two anode variables fixed (Figure 4-9 to Figure 4-32). From these figures, it is obvious that D_a and L_a affect the resistances more than d and H_a do. Particularly, for the relationship between the scaled resistance and the normalized diameter of anode for different lengths of anode, the three curves intersect at the section of larger diameter of anode because the scaled resistance decreases at the section of smaller length of anode when normalized diameter of anode is large.

Stray Current Modeling

As is discussed in Chapter 2, corrosion caused by stray current effects may be observed in cathodic protection systems. The corrosion level on the pipes depends on the coating properties of the pipes. In CP3D software, four typical coating properties are involved which are shown in Table 4-2, especially, for the pipes with coating A (aged bare steel pipe) and coating B (fresh bare steel pipe), there are actually no coating films present on the surface of the pipes. Two kinds of stray current effects were modeled: 1) stray current effects due to a single anode; and 2) stray current effects due to an anode bed.

Stray Current Effects Due to a Single Anode

Table 4-3 shows the configuration of the pipes in a stray-current-effect system due to a single anode. The anode which was connected to the protected pipe had dimensions: L_a =0.5m, D_a =0.2m, H_a =1m, d =10m, and was considered to be impressed current anode with an applied voltage of 8V. The visual configuration is

shown in Figure 4-33. The blue pipe represents the protected pipe; whereas, the red pipe represents the unprotected pipe. From Figure 4-33, it is clearly seen that stray currents which came from the anode were picked by the unprotected pipe (foreign pipe). The potential and current density distribution along the unprotected pipe are shown in Figures 4-34 and 4-35 respectively. The valleys both in the two figures are related to the site at the foreign pipe where stray currents from the anode entered. A peak in Figure 4-35 can be clearly seen at the site of unprotected pipe which is associated with the cross-over section of two pipes. A close-up profile is shown in Figure 4-36. The peak represents section where stray currents exited the unprotected pipe. Thus, this section tends to be more corrosive than the other sections along the unprotected pipe.

Stray Current Effects Due to an Anode Bed

The configuration of this stray-current-effect system due to an anode bed is shown in Table 4-4. Each anode in the anode bed had the dimensions: L_a =0.5m, D_a =0.2m, H_a =1m, $d_{1,2,3}$=0.012m, 0.016m, 0.02m, and was considered to be impressed current anode with impressed voltage of 4V. A visual configuration is shown in Figure 4-37, where the blue pipe represents the protected pipe and the red one represents the unprotected pipe. The potential and current density distributions along the unprotected pipe are shown in Figures 4-38 and 4-39 respectively. Just like the analysis for stray current effects due to a single anode, the valleys both in the two figures are related to the site at the unprotected pipe where stray currents from the anode bed came in, and the peak in Figure 4-40 represents the site where stray currents exited the unprotected pipe. This section is also more corrosive than the other sections along the unprotected pipe.

Rectifier War Modeling

The method of modeling stray current effects was extended to a more complex situation: rectifier wars. The rectifier war is a term of describing corrosion happened between two cathodic protection systems. It is caused by the potential difference of the cathodic protection of two pipes. Here, the criterion that -850mV CSE ≤ V≤ -1200mV CSE for adequate cathodic protection was applied.

Rectifier Wars in Soil Environment

.For the purpose of the present calculations, the rectifier war modeling in a soil environment started with condition 1. The configuration of condition 1 is shown in Table 4-5. The two pipes in condition 1 had the same properties and experienced the same cathodic protection. The corresponding visual configuration is shown in Figure 4-41. The potential and current density distributions along pipe 1 and pipe 2 in condition 1 were obtained by CP3D calculations. For pipe 1, a comparison of the potential and current density distributions before and after introducing pipe 2 is shown in Figures 4-42 and 4-43 respectively. The valleys that appear in both figures were associated to the site of pipe where anodes were connected. The peaks indicate the interference between two pipes, but the interference was not very strong because the potential difference of the peak is small in Figure 4-42. A comparison of potential and current distributions between pipe 1 and pipe 2 are shown in Figures 4-44 and 4-45, respectively. These two figures indicate that pipe 1 and pipe 2 nearly experience the same cathodic protection.

Then, condition 1 was changed to condition 2, where the impressed voltage of cathodic protection on pipe 1 was increased to 5.8V, and cathodic protection on pipe 2 was fixed. The new potential and current density distributions in condition 2 are shown in Figures 4-46 and 4-47, respectively. These two figures indicate that pipe 1

experienced more cathodic protection than did pipe 2, since the potential and current density distributions along pipe 1 were more negative than that along pipe 2. In condition 2, corrosion began to occur on the site of pipe 2 which is associated with the cross-over section. This point can be clearly illustrated by Figure 4-48, which provides a comparison of potential distributions of pipe 2 in two conditions. The peak, which was above -850mV CSE in condition 2 plot, indicates that the cathodic protection difference between the two pipes may result in the localized corrosion on the pipe which has less cathodic protection at the cross-over section.

Rectifier Wars in Seawater Environment

For the purpose of the present calculations, the rectifier war modeling in seawater environment started with condition 1. The configuration of condition 1 is shown in Table 4-6. In condition 1, only pipe 1 was installed in the system, and two anodes with impressed voltages of 7.3V provided cathodic protection to pipe 1. For condition 2, pipe 2 was introduced to the system which also was connected to two anodes with impressed voltages of 7.3V. Finally, condition 2 was changed to condition 3. In condition 3, the potentials of the anodes connected to pipe 2 was increased to 10V, while the potentials of the anodes connected to pipe 1 remained at 7.3V. The process of this modeling is shown in Figure 4-49. Here only the current density and potential distributions of pipe 1 (Figures 4-50 and 4-51) were taken into account since they showed directly the localized corrosion due to the rectifier war. In Figure 4-51, the potential peaks in condition 2 and 3 were both above the level of -850mV CSE, which indicate localized corrosion. Also the current densities in conditions 2 and 3 were more positive than in condition 1 at peak area in Figure 4-51. These two figures indicate that: 1) introducing pipe 2 will result in localized corrosion on the pipe 1 at the cross-over

sections, and the corrosion is caused by interference between two pipes. 2) Increasing cathodic protection on pipe 2 will intensify localized corrosion that has already occuring on the pipe 1. This point can be further illustrated by Figure 4-52.

Anode Distribution

It is important to understand the anode distribution for a certain length of pipe. The most important factor in the determination of anode distribution is the number of anodes. Inadequate numbers of anodes will result in corrosion of the pipe; whereas, superfluous anodes, especially impressed current anodes will result in unnecessary energy loss. Thus, it is essential to determine the minimum number of anodes required to provide sufficient cathodic protection.

Anode Distribution in Soil Environment

The first step to establish an anode distribution model was to specify the base conditions. The dimensional analysis indicated that the current density distribution is affected by the soil resistivity and anode properties. Thus, in this model, the base conditions were: ρ = 10,000 ohm-cm, L_a = 1m, D_a = 0.1m, H_a = 1m and d = 40m. The anode used in this model was a high-performance Magnesium anode. The pipe dimensions were: D_L = 0.3m and H_L = 1m. The coating property of the pipe was Coating C.

The second step was to calculate the current output from the single anode, which can be obtained by applying Dwight's formula

$$R_{\text{Anode}} = \left(\frac{0.005 \times 10000}{\pi \times 1}\right)\left(\ln\frac{8 \times 1}{0.1} - 1\right) = 53.82\text{ohm} \quad (4\text{-}8)$$

The potential range for a system under adequate cathodic protection is -850 mV CSE to -1200mV CSE. This means that the critical value of the off potential is -850 mV CSE in

order to get minimum number of anodes. The corresponding driving potential for activation of the cathodic protection was

$$V_{\text{driving potential}} = \text{-}1.75\text{V} - (-\,0.85\text{V}) = -\,0.9\text{V} \tag{4-9}$$

Thus, the current output from a single anode is

$$I_{\text{anode}} = \left| \frac{V_{\text{driving potential}}}{R_{\text{anode}}} \right| = \left| \frac{-\,0.9}{53.82} \right| \text{A} = 0.0167\text{A} \tag{4-10}$$

The third step was to calculate the total current required to protect the pipe. The equation for calculation of total current was written as

$$I_{\text{total}} = \frac{\text{A} \times i}{0.9} = \frac{\pi \times L \times D_{\text{L}} \times i}{0.9} = 1.047 L \times i \tag{4-11}$$

where A is the total area of pipe, i is the current density and L is the length of the pipe. Finally, the minimum number of anodes required was written as

$$N_{\text{minimun}} = \frac{I_{\text{total}}}{I_{\text{anode}}} = \frac{1.047 L \times i}{0.0167} \tag{4-12}$$

The current density, i, can be obtained by implementing CP3D simulation. For a pipe with a length of 18,300m, at least two anodes were needed to obtain potential range which was close to a critical value of -850mV CSE. The off-potential distribution along the pipe is shown in Figure 4-53. The corresponding minimum current density for Poor 20mil FBE pipe was

$$i = \frac{2 \times 0.0167}{1.047 \times 18{,}300} = 1.743 \times 10^{-6}\,\text{A/m}^2 \tag{4-13}$$

In order to verify accuracy of the value of the minimum current density, the results obtained by implementing CP3D software were compared with those obtained by applying Dwight's formula, shown in Table 4-7. Figure 4-54 gives a vivid comparison

between the CP3D simulation and the Dwight's formula. It is observed that the plots of these two methods almost overlap. In conclusion, the minimum current density required to protect Poor 20mil FBE pipe is $1.743\times10^{-6}\,\mathrm{A/m^2}$ under the initial conditions specified.

Anode Distribution in Seawater Environment

The base condition for anode-distribution-determination model in seawater environment was different from that in soil environment: ρ = 20 ohm-cm, L_a =1m, D_a =0.1m, H_a = 1m and d = 40m. The anode used in this model was an impressed current anode with impressed potential of 4V. So for the pipe, D_L = 0.3m, H_L = 1m, and the coating property of the pipe was Coating A. Here the limiting current density for oxygen reduction of Coating A was changed to 9 $\mu\mathrm{A/cm^2}$ in seawater environment.

The second step was to calculate the current output from the single anode using the Dwight formula

$$R_{\mathrm{Anode}}=\left(\frac{0.005\times20}{\pi\times1}\right)\left(\ln\frac{8\times1}{0.1}-1\right)=0.10765\mathrm{ohm} \qquad (4\text{-}14)$$

An impressed voltage of 4V was provided by a rectifier in the cathodic protection system, but the effective potential added between the anode and the protected pipe was less than 4V. This result can be explained by using CP3D. For the same configuration of cathodic protection system, when impressed voltage decreased to 0, the potential difference between the anode and the pipe was equal to (-0.85-0.382) V, and the anode became the cathode in the electrochemical system. This result shows that, if 4V was applied, the actual driving potential between the anode and the pipe was: (4 - 0.85 - 0.382) V – 0.85V= 1.918V. Thus, the current output from a single anode was

$$I_{\text{anode}} = \left| \frac{V_{\text{driving potential}}}{R_{\text{anode}}} \right| = \left| \frac{1.918}{0.10765} \right| \text{A} = 18.72\text{A} \tag{3-10}$$

This result is used to estimate the minimum numbers of anodes.

The third step was to calculate the minimum current density needed. Using the same strategy in anode distribution in soil environment, the minimum current density in this situation was 0.08A/m^2. In order to verify the accuracy of the value of this minimum current density, the result obtained by implementing CP3D software was compared with those by applying the Dwight's formula as is shown in Table 4-8. Figure 4-55 also gives a comparison between CP3D simulation and Dwight's formula in seawater condition. It is evident that the plots of these two methods overlap. In conclusion, the minimum current density required to protect aged bare steel pipe is 0.08A/m^2 under the base condition specified.

Table 4-1. List of variables affecting current distribution along a pipe

Parameter	Definition
L	Length of the single pipe
D_L	Diameter of the single pipe
H_L	Depth of the single pipe
L_A	Length of the anode
D_A	Diameter of the anode
H_A	Depth of the anode
D	Distance between the single pipe and the anode
R	Resistance of the anode and single pipe system
P	Soil resistivity

Table 4-2. Physical and chemical properties of four different types of coatings

Coating property	Coating A	Coating B	Coating C	Coating D
Coating Resistivity*10^8 (ohm-cm)	-	-	2	50
Coating Thickness (mm)	-	-	0.508	0.508
Oxygen Blocking (%)	-	-	99	99.9
Corrosion Potential (mV CSE)	-520.7	-457.4	-635.7	-654.3
E_{Fe} (mV CSE)	-522	-522	-522	-522
β_{Fe} (mV/ decade)	59	62.6	62.6	62.6
I_{O2} ($\mu A/cm^2$)	1.05	10.76	1.05	1.05
E_{O2} (mV CSE)	-172	-172	-172	-172
β_{O2} (mV/ decade)	61	66.5	66.5	66.5
E_{H2} (mV CSE)	-942	-942	-942	-942
β_{H2} (mV/ decade)	132.1	132.1	132.1	132.1

Table 4-3. Configuration of two pipes in stray current effect system due to a single anode

	L	D_L	H_L	Coating property
Protected pipe	100m	0.3m	1m	Coating C
Unprotected pipe	1,000m	0.3m	1m	Coating A

Table 4-4. Configuration of two pipes in stray current effect system due to an anode bed

	L	D_L	H_L	Coating property
Protected pipe	200m	0.3m	1m	Coating C
Unprotected pipe	1,000m	0.3m	1m	Coating A

Table 4-5. Configuration of condition 1 for rectifier war in soil environment

	L	Coating property	Initial anode type	Soil resistivity
Pipe 1	1,000m	Coating C	Iccp 1.35V	10,000ohm-cm
Pipe 2	1,000m	Coating C	Iccp 1.35V	

Table 4-6. Initial configuration of two pipes for rectifier war in seawater environment

	L	Coating property	Initial anode type	Seawater resistivity
Pipe 1	1,000m	Coating A	2 Iccp 7.3 V	10,000ohm-cm
Pipe 2	1,000m	Coating A	2 Iccp 7.3 V	

Table 4-7. Comparison between CP3D and Dwight's Formula in soil environment

	Length of the pipe	$N_{min,anode}$ (CP3D)	$N_{min,anode}$ (Dwight)
1	9km	1	0.98
2	18km	2	1.96
3	27km	3	2.95
4	36km	4	3.93
5	45km	5	4.91
6	54km	6	5.89
7	63km	7	6.84
8	72km	8	7.86
9	81km	9	8.84
10	90km	10	9.82

Table 4-8. Comparison between CP3D and Dwight's formula in seawater environment

	Length of the pipe	$N_{min,anode}$ (CP3D)	$N_{min,anode}$ (Dwight)
1	212m	1	0.997
2	425m	2	1.998
3	638m	3	2.999
4	850m	4	3.996
5	1,063m	5	4.997
6	1,276m	6	5.999
7	1,488m	7	6.995
8	1,701m	8	7.997
9	1,914m	9	8.998
10	2,127m	10	10.000

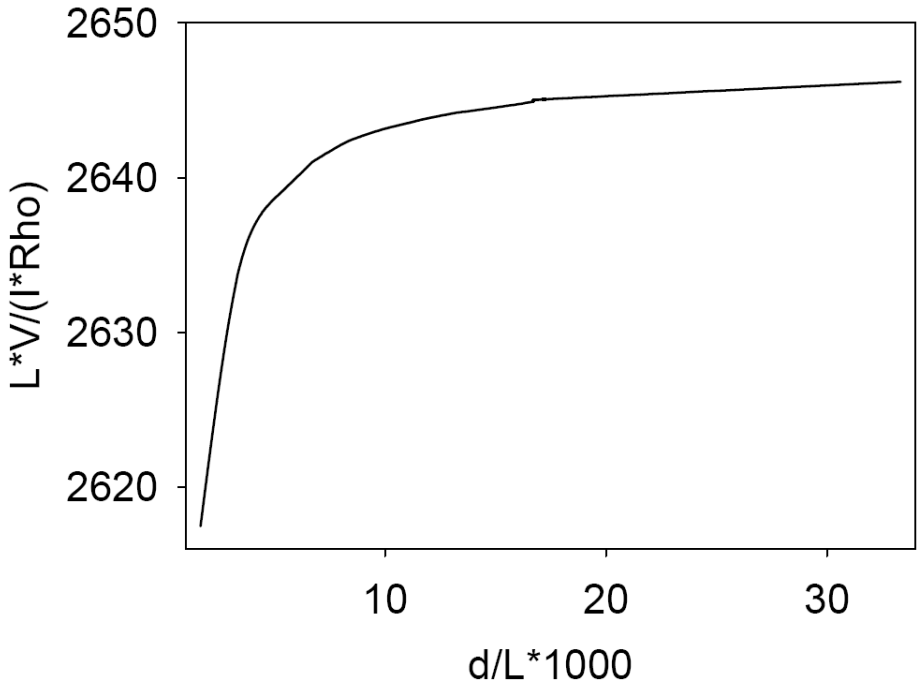

Figure 4-1. Normalized resistance as a function of normalized anode distance

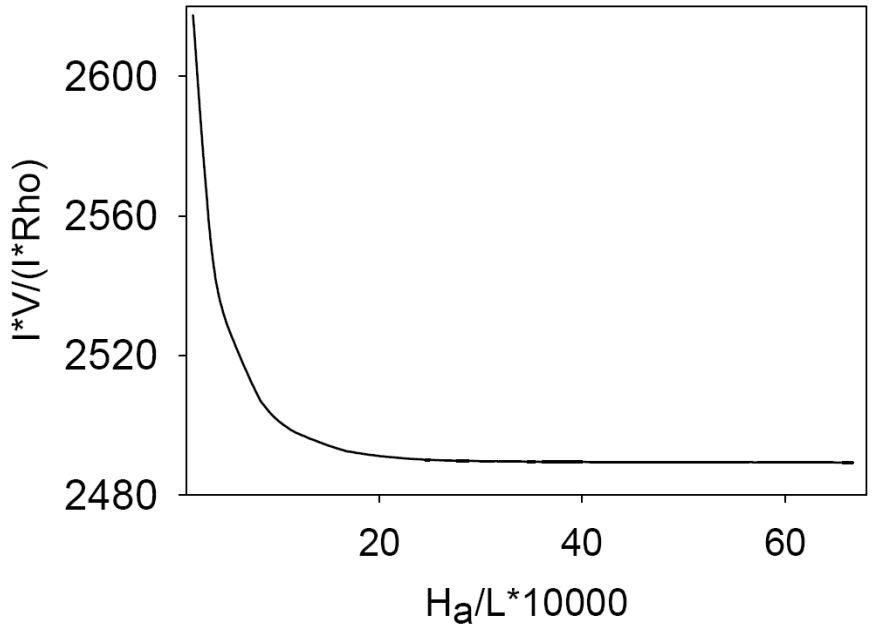

Figure 4-2. Normalized resistance as a function of normalized depth of anode

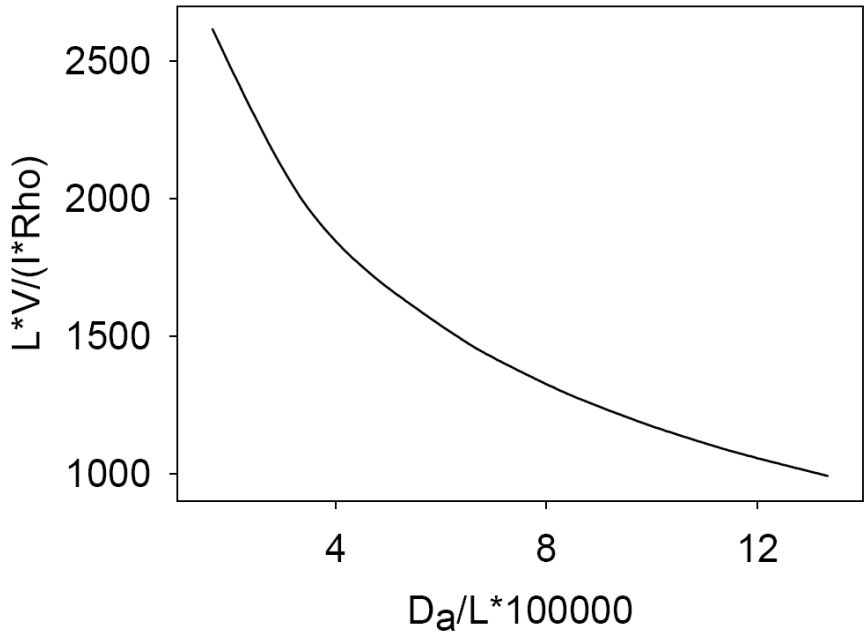

Figure 4-3. Normalized resistance as a function of normalized diameter of anode

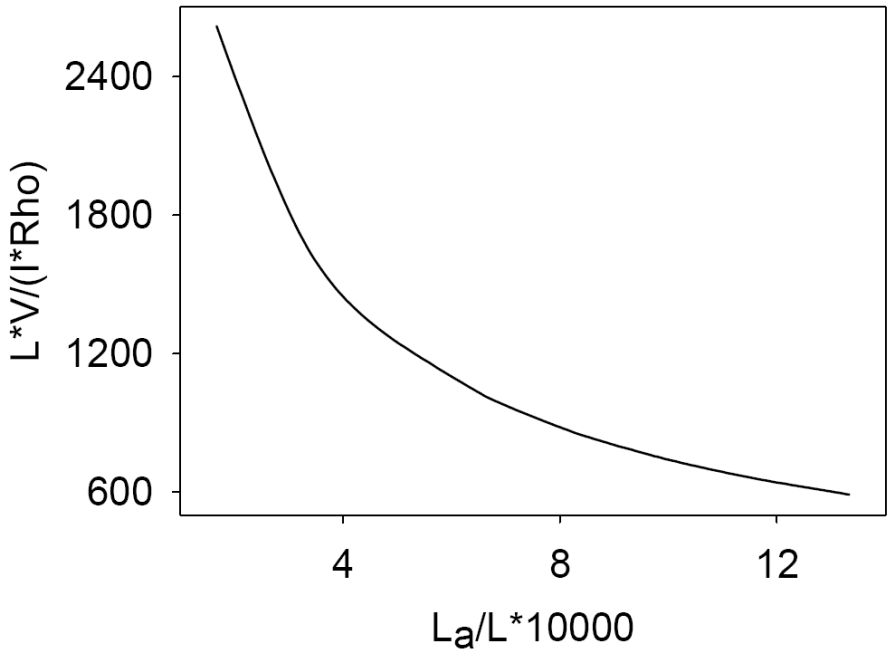

Figure 4-4. Normalized resistance as a function of normalized length of anode

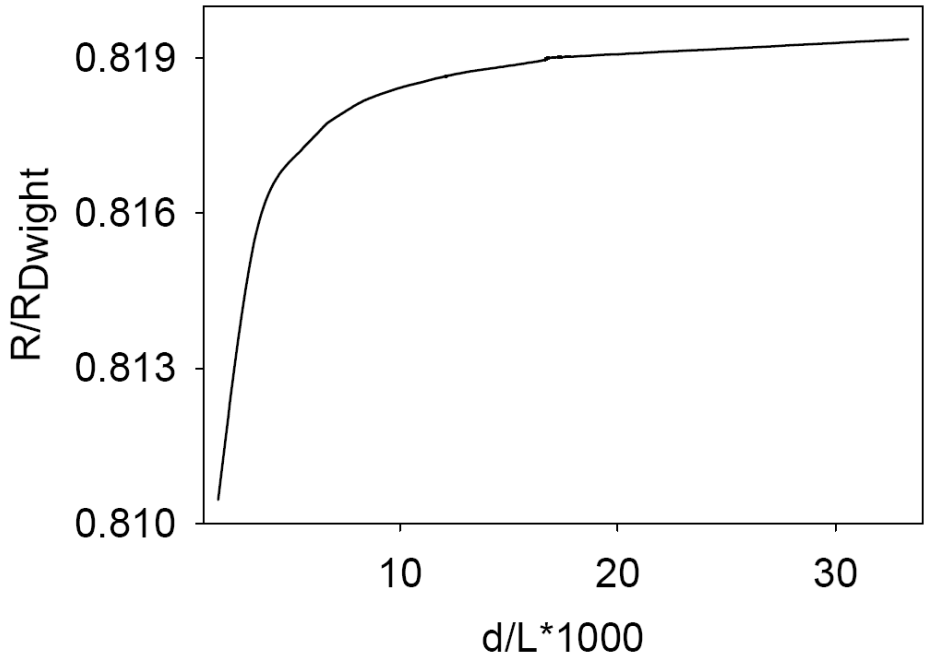

Figure 4-5. Scaled resistance as a function of normalized anode distance

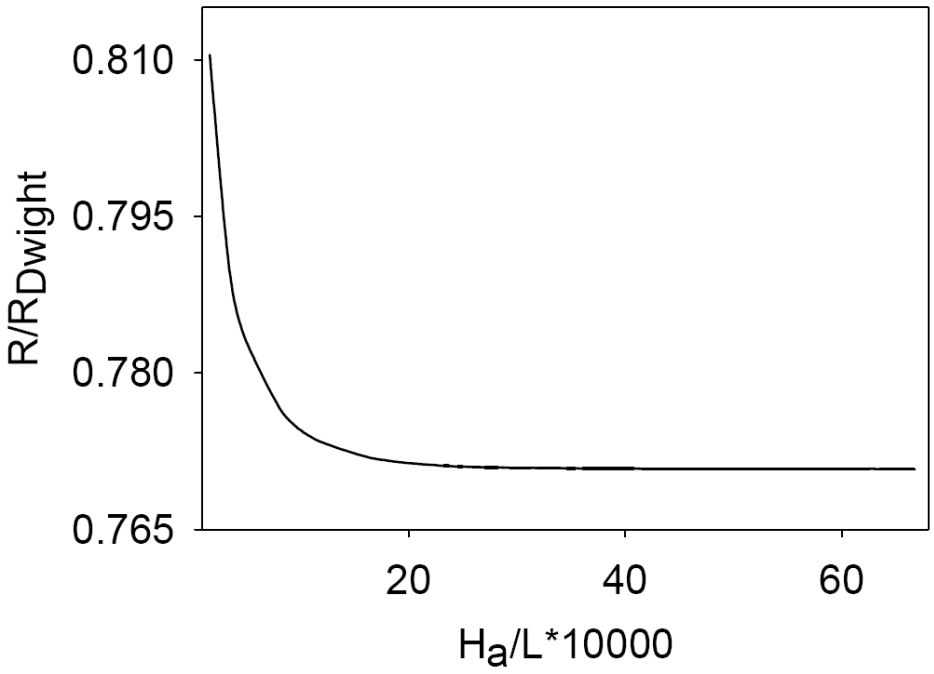

Figure 4-6. Scaled resistance as a function of normalized depth of anode

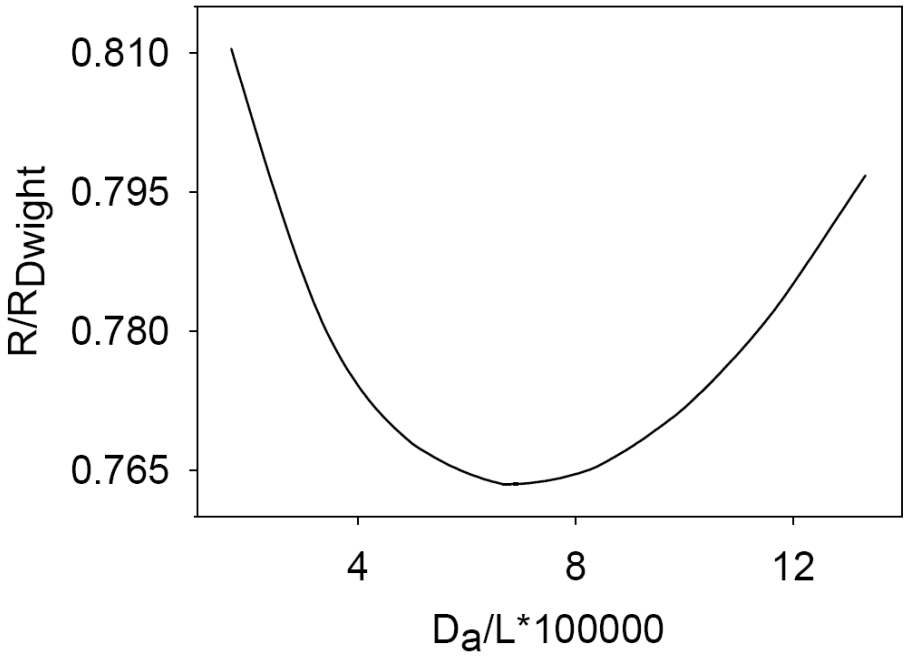

Figure 4-7. Scaled resistance as a function of normalized diameter of anode

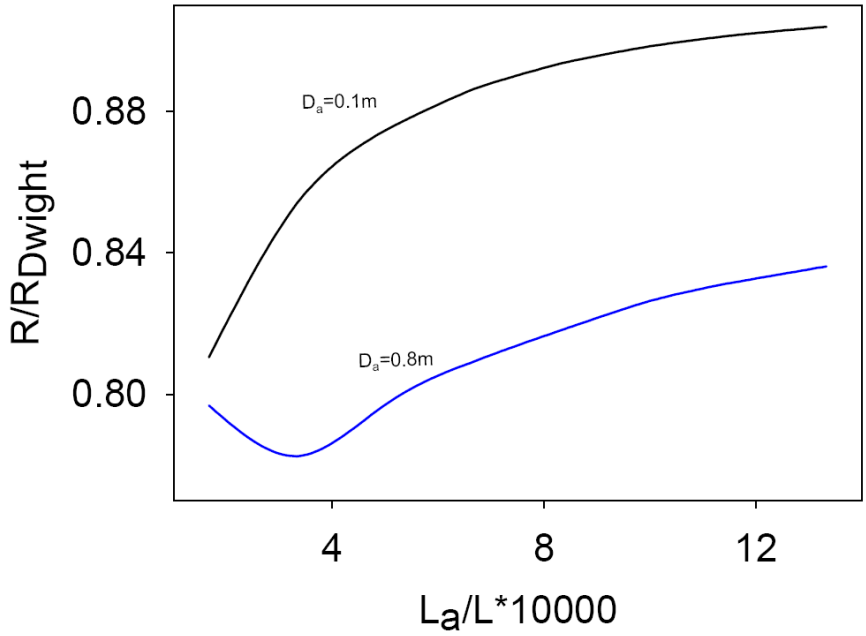

Figure 4-8. Scaled resistance as a function of normalized length of anode in different anode-diameter conditions.

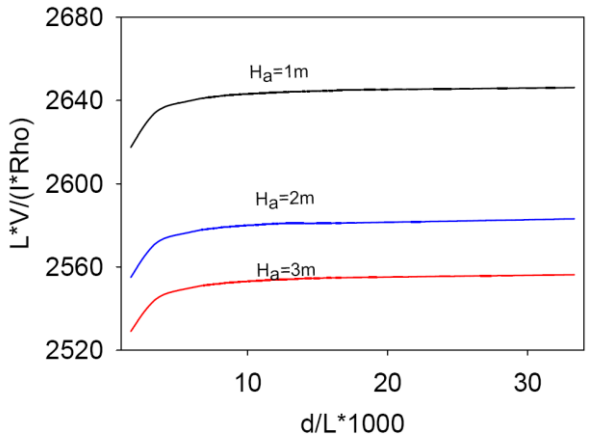

Figure 4-9. Normalized resistance as a function of normalized anode distance with normalized depth of anode as a parameter

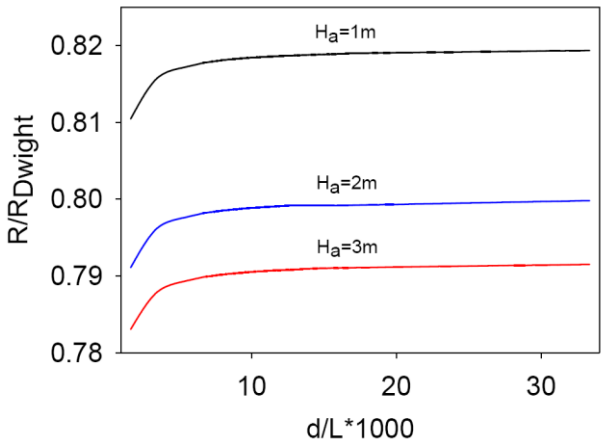

Figure 4-10. Scaled resistance as a function of normalized anode distance with scaled depth of anode as a parameter

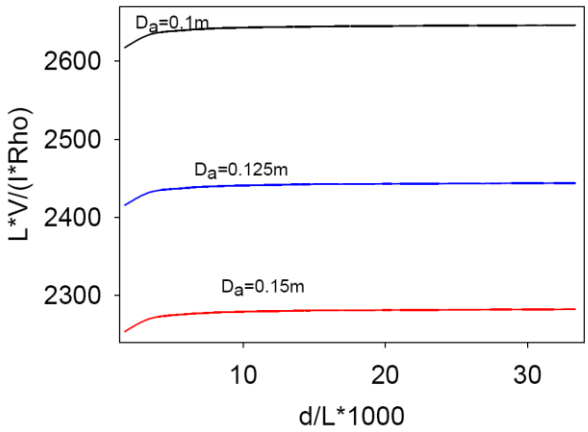

Figure 4-11. Normalized resistance as a function of normalized anode distance with normalized diameter of anode as a parameter

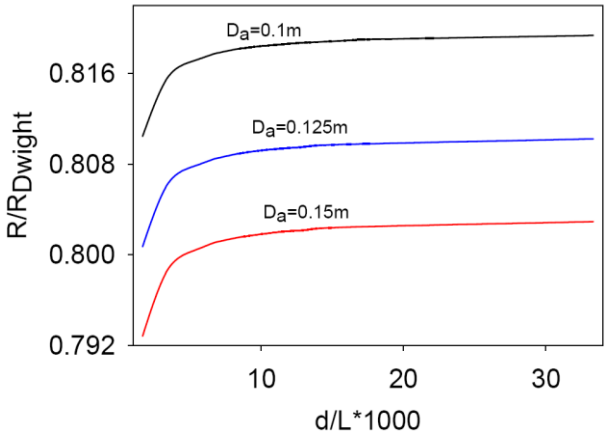

Figure 4-12. Scaled resistance as a function of normalized anode distance with normalized diameter of anode as a parameter

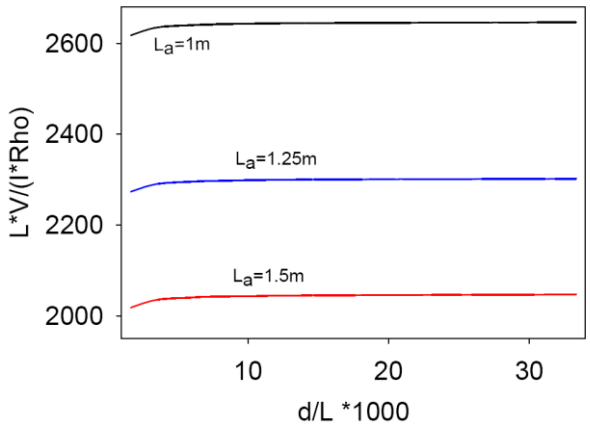

Figure 4-13. Normalized resistance as a function of normalized anode distance with normalized length of anode as a parameter

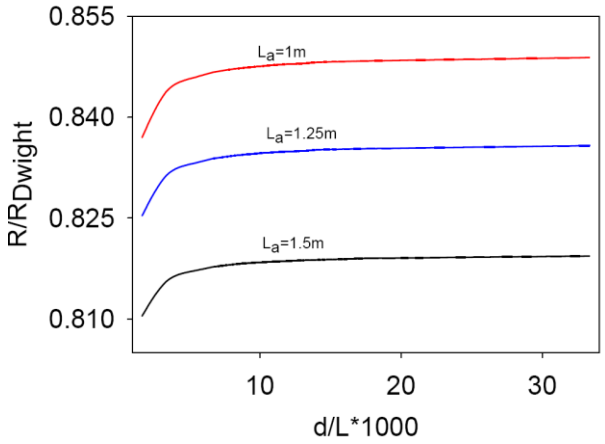

Figure 4-14. Scaled resistance as a function of normalized anode distance with normalized length of anode as a parameter

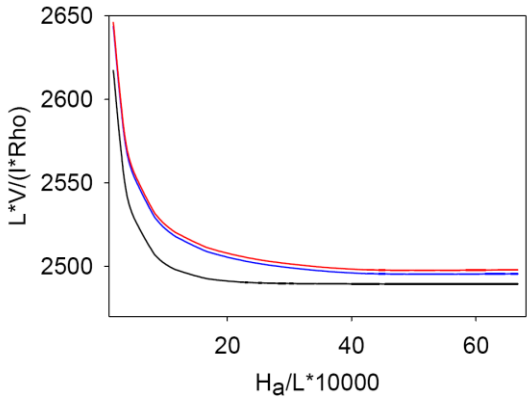

Figure 4-15. Normalized resistance as a function of normalized depth of anode with normalized anode distance as a parameter. The black line: d=10m; blue line d=70m, red line: d=200m.

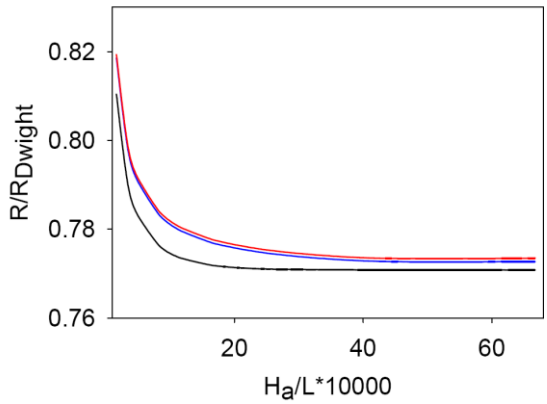

Figure 4-16. Scaled resistance as a function of normalized depth of anode with normalized anode distance as a parameter. The black line d=10m; blue line: d=70m, red line: d=200m.

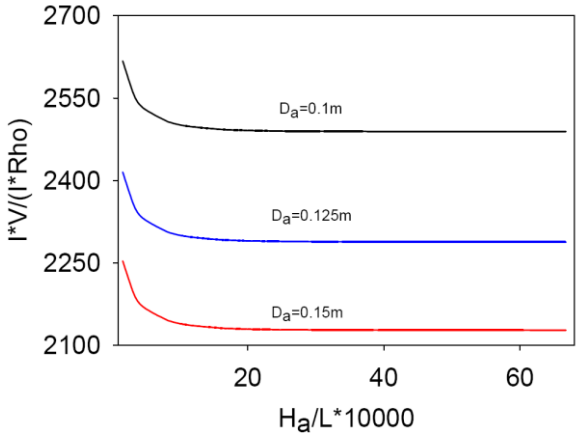

Figure 4-17. Normalized resistance as a function of normalized depth of anode with normalized diameter of anode as a parameter

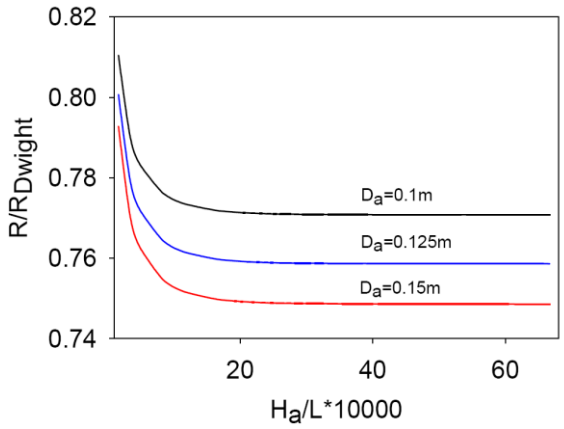

Figure 4-18. Scaled resistance as a function of normalized depth of anode with normalized diameter of anode as a parameter

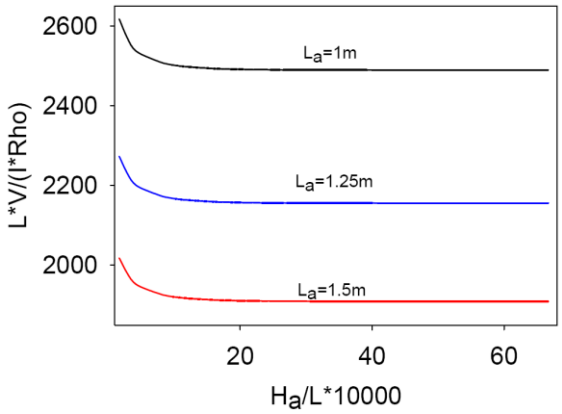

Figure 4-19. Normalized resistance as a function of normalized depth of anode with normalized length of anode as a parameter

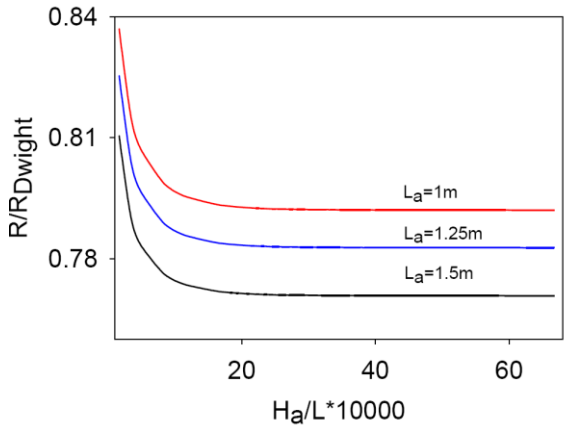

Figure 4-20. Scaled resistance as a function of normalized depth of anode with normalized length of anode as a parameter

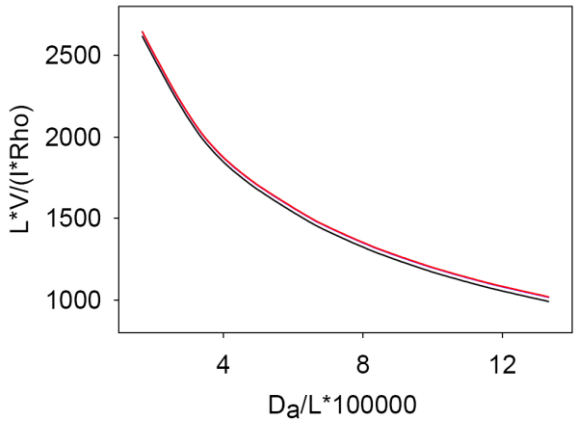

Figure 4-21. Normalized resistance as a function of normalized diameter of anode with normalized anode distance as a parameter. Black line: d=10m; blue line: d=70m, red line: d=200m

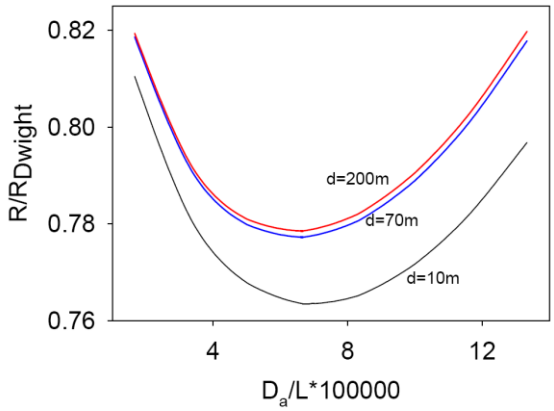

Figure 4-22. Scaled resistance as a function of normalized diameter of anode with normalized anode distance as a parameter

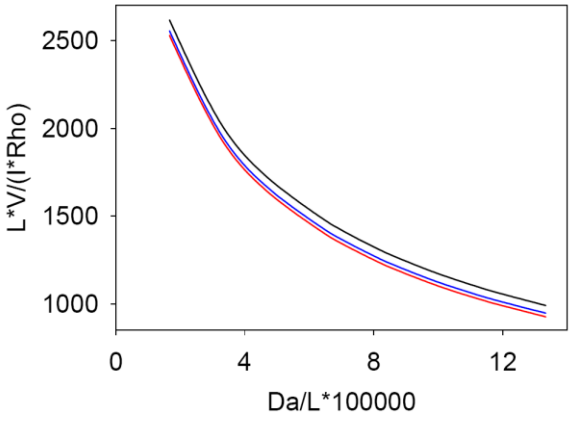

Figure 4-23. Normalized resistance as a function of normalized diameter of anode with normalized depth of anode as a parameter. Black line: H_a=1m; blue line: H_a=2m, red line: H_a=3m

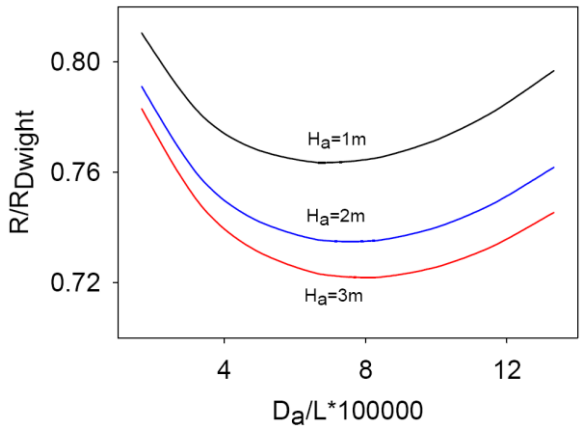

Figure 4-24. Scaled resistance as a function of normalized diameter of anode with normalized depth of anode as a parameter

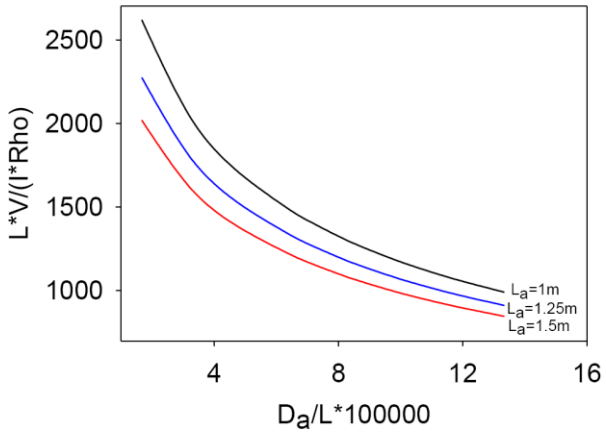

Figure 4-25. Normalized resistance as a function of normalized diameter of anode with normalized length of anode as a parameter

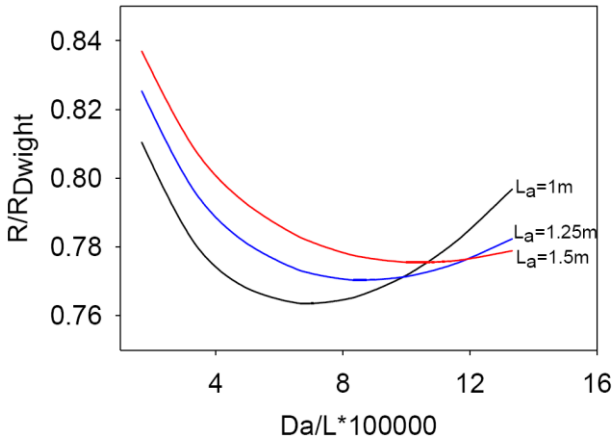

Figure 4-26. Scaled resistance as a function of normalized diameter of anode with normalized length of anode as a parameter

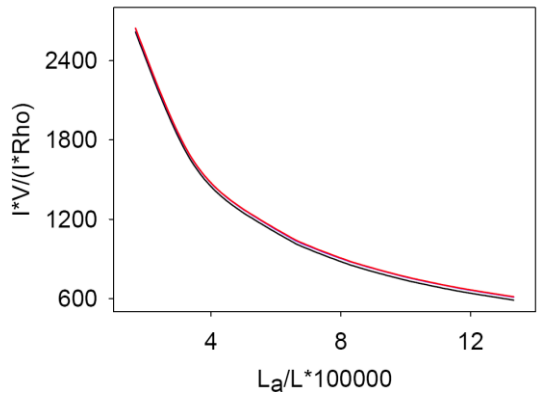

Figure 4-27. Normalized resistance as a function of normalized length of anode with normalized anode distance as a parameter. Black line: d=10m; blue line: d=70m; red line: d=200m

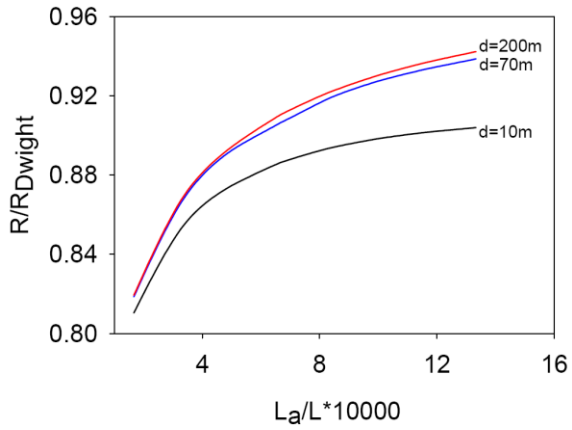

Figure 4-28. Scaled resistance as a function of normalized length of anode with normalized anode distance as a parameter

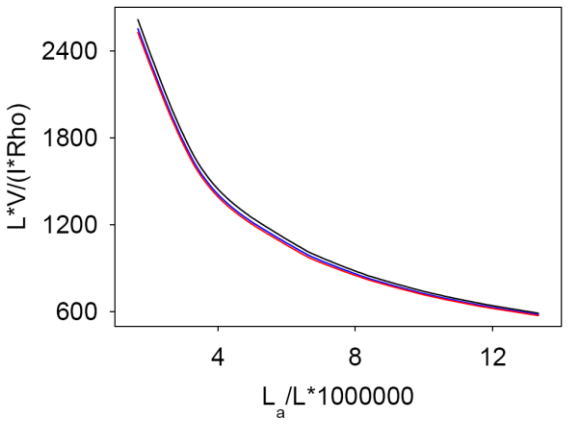

Figure 4-29. Normalized resistance as a function of normalized length of anode with normalized depth of anode as a parameter. Black line: H_a=1m, blue H_a=2m, red H_a=3m

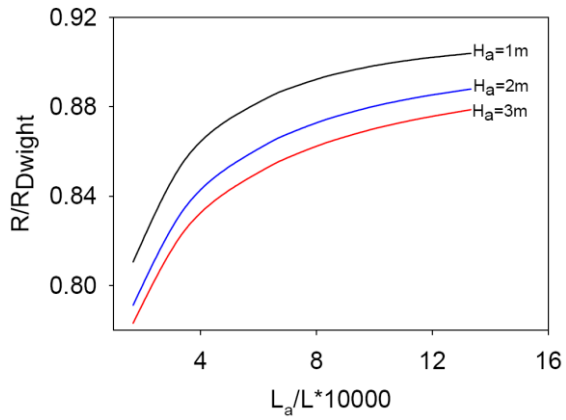

Figure 4-30. Scaled resistance as a function of normalized length of anode with normalized depth of anode as a parameter

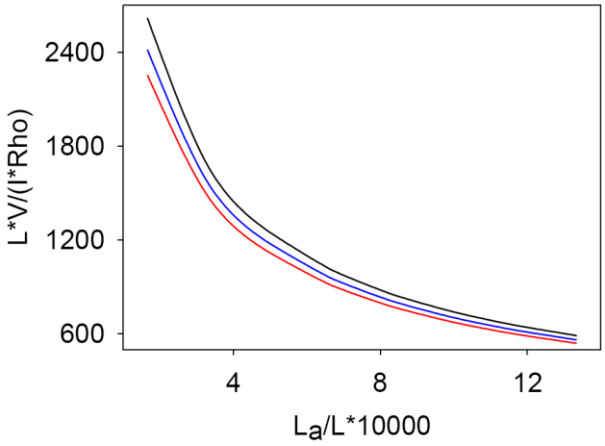

Figure 4-31. Normalized resistance as a function of normalized length of anode with normalized diameter of anode as a parameter. Black line: D_a=0.1m; blue line: D_a=0.125m; red line: D_a=0.15m.

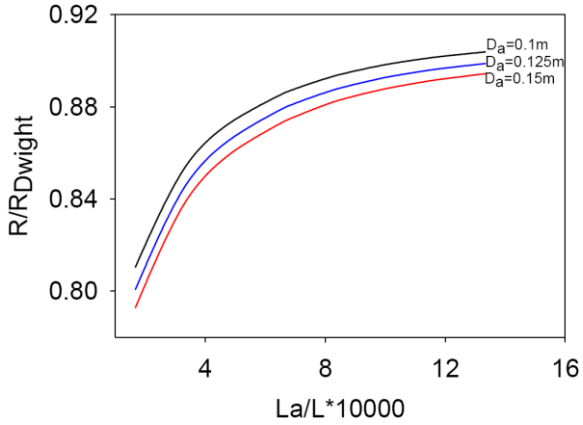

Figure 4-32. Scaled resistance as a function of normalized length of anode with normalized diameter of anode as a parameter

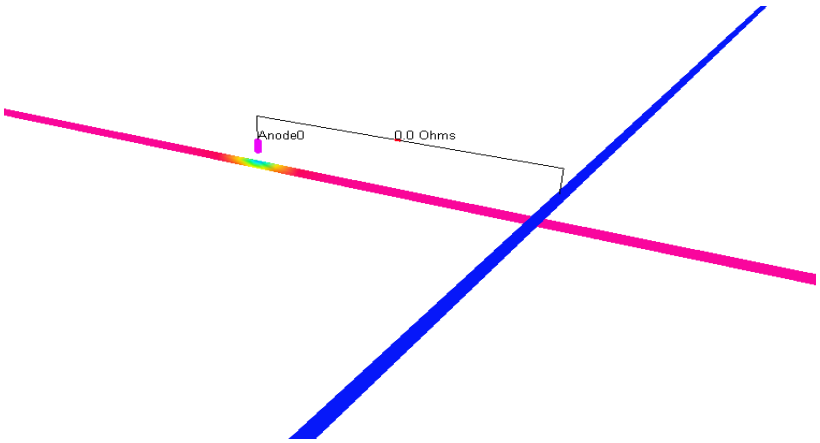

Figure 4-33. Configuration of stray-current-effect system due to a single anode

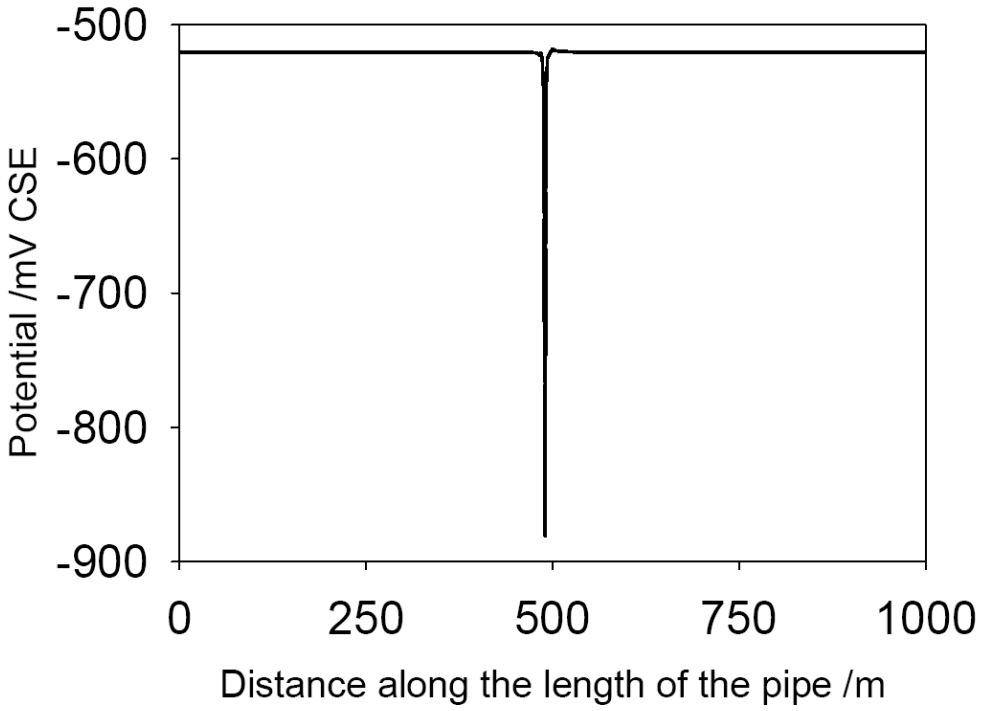

Figure 4-34. Potential distribution along the unprotected pipe in a stray-current-effect system due to a single anode

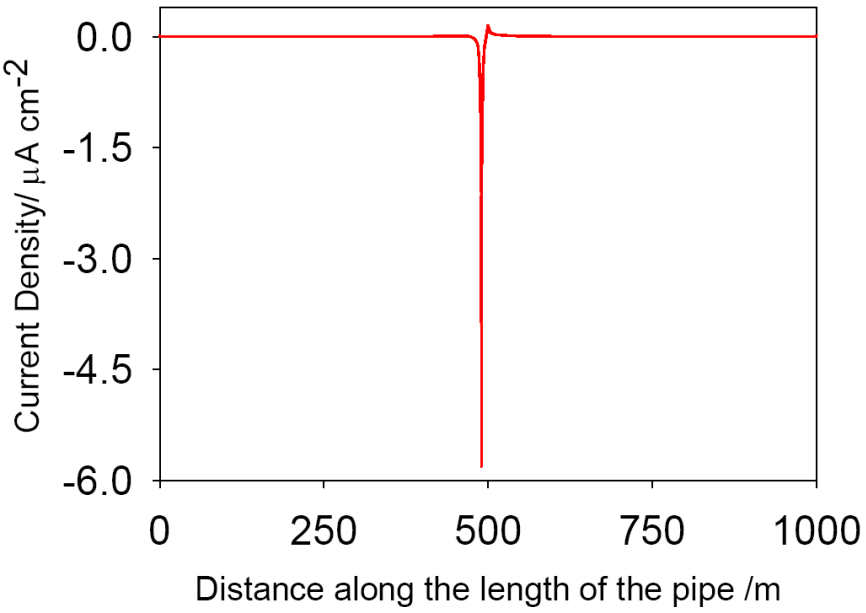

Figure 4-35. Current density distribution along the unprotected pipe in a stray-current-effect system due to a single anode

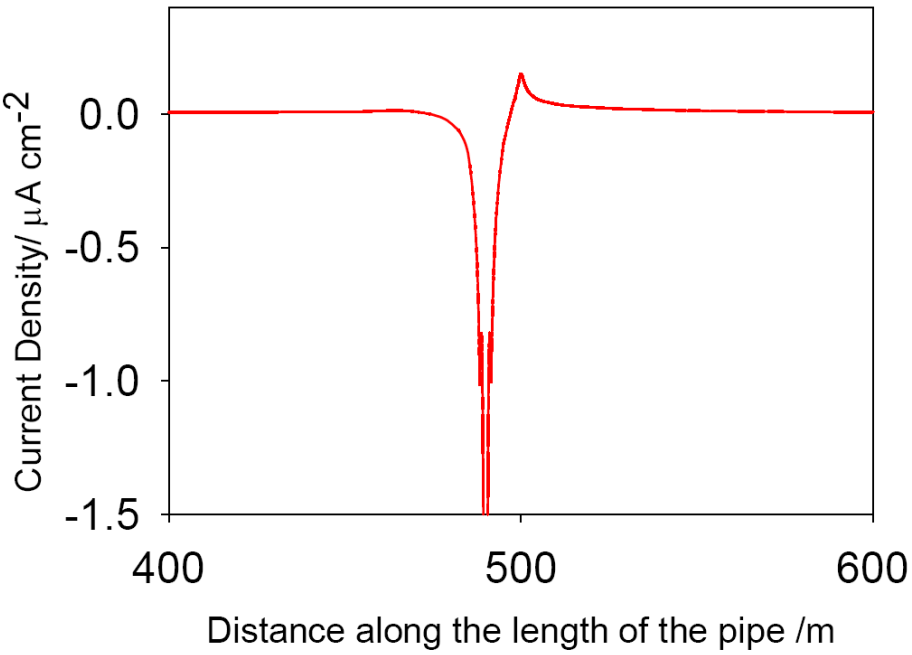

Figure 4-36. A close up of current density distribution along the interested section of the unprotected pipe in a stray-current-effect system due to a single anode

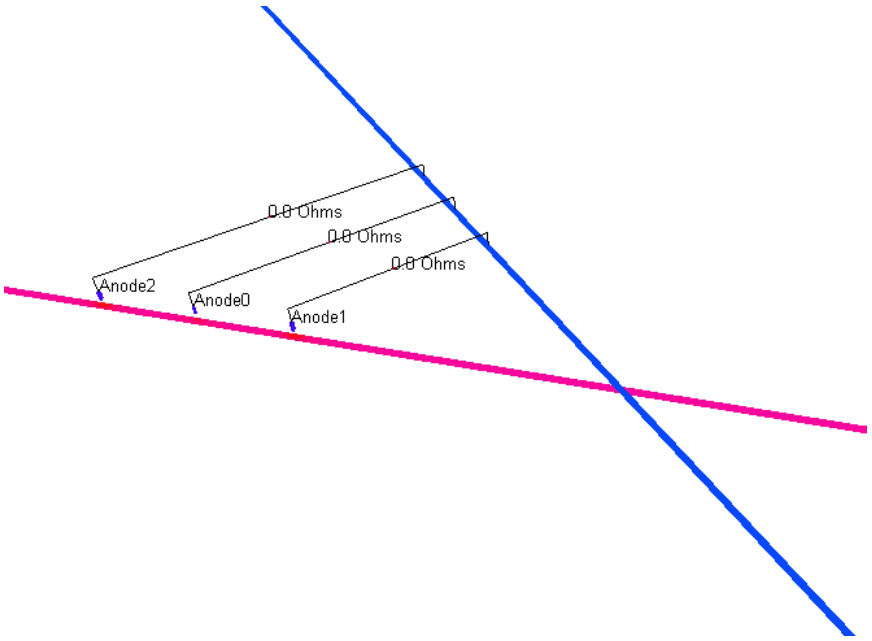

Figure 4-37. Configuration of stray-current-effect system due to an anode bed

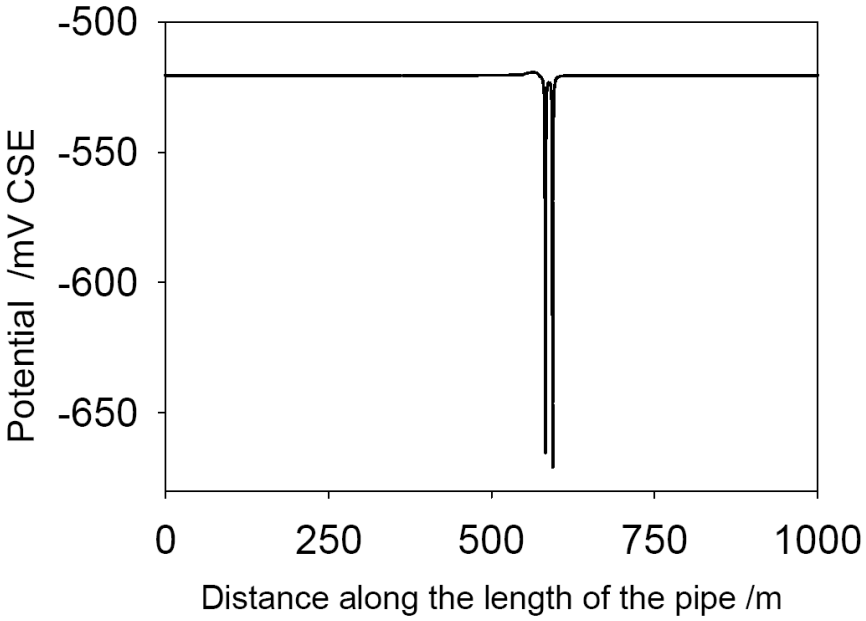

Figure 4-38. Potential distribution along the unprotected pipe in a stray-current-effect system due to an anode bed

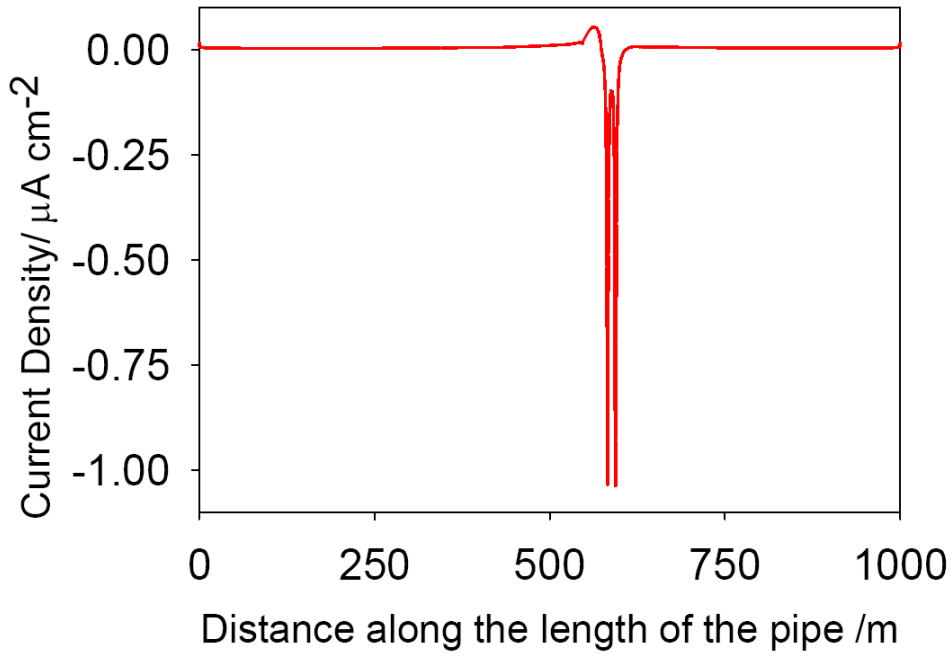

Figure 4-39. Current density distribution along the unprotected pipe in a stray-current-effect system due to an anode bed

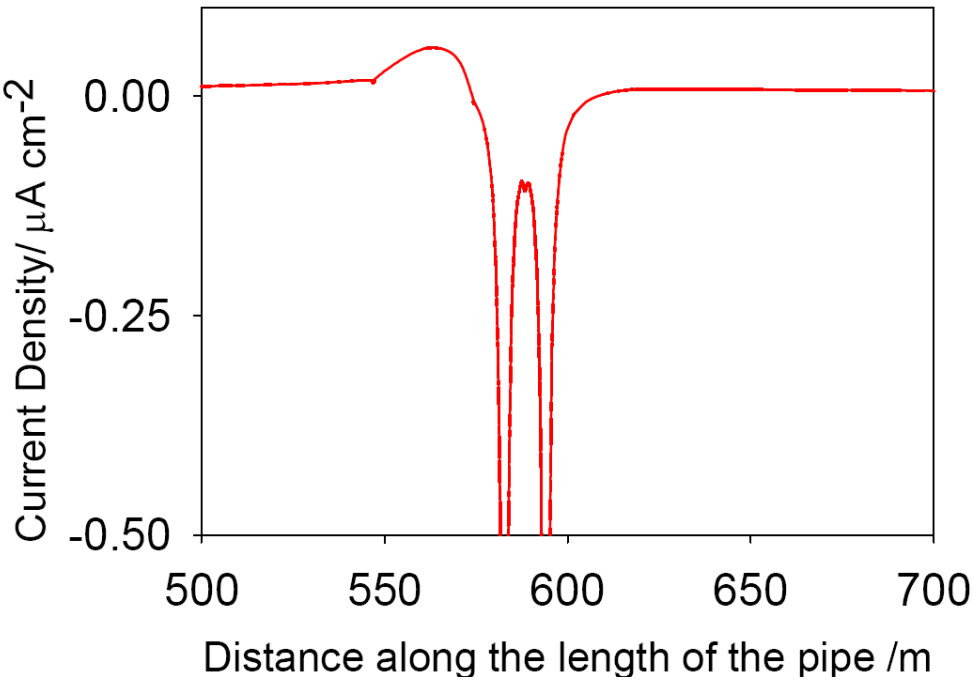

Figure 4-40. A close-up of current density distribution along the interested section of the unprotected pipe in a stray-current-effect system due to an anode bed

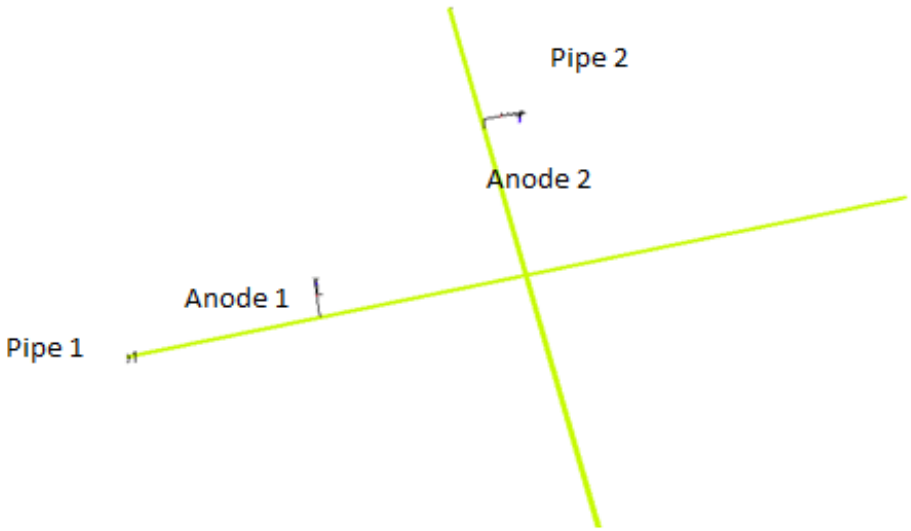

Figure 4-41. Configuration of condition 1 for rectifier war modeling in soil environment

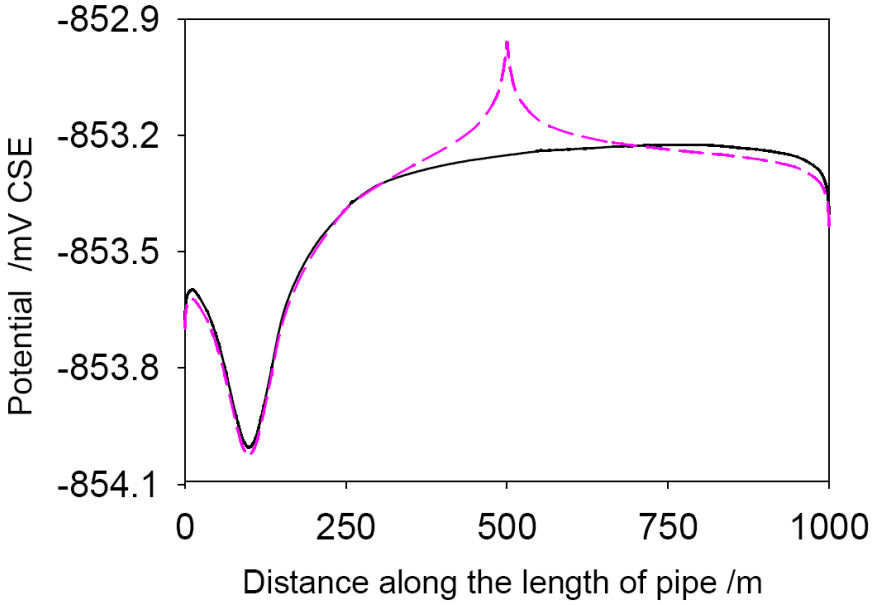

Figure 4-42. Comparison of potential distributions along pipe 1 before and after introducing pipe 2. Black solid line: before introducing pipe 2; Rose red dash line: after introducing pipe 2

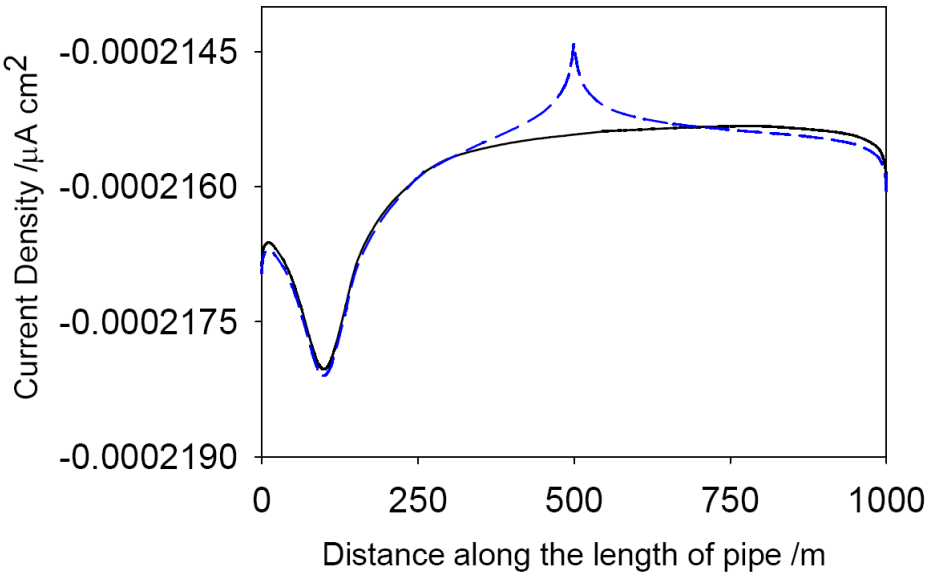

Figure 4-43. Comparison of current density distributions along pipe 1 before and after introducing pipe 2. Black solid line: before introducing pipe 2; blue dash line: after introducing pipe 2

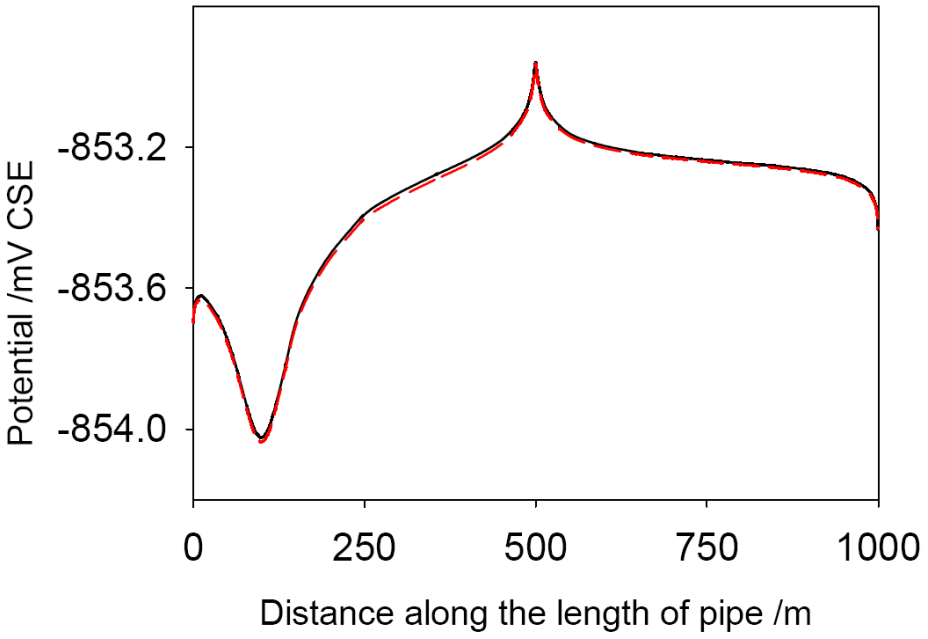

Figure 4-44. Comparison of potential distributions along pipe 1 and pipe 2 respectively in condition 1. Black solid line: pipe 1; red dash line: pipe 2

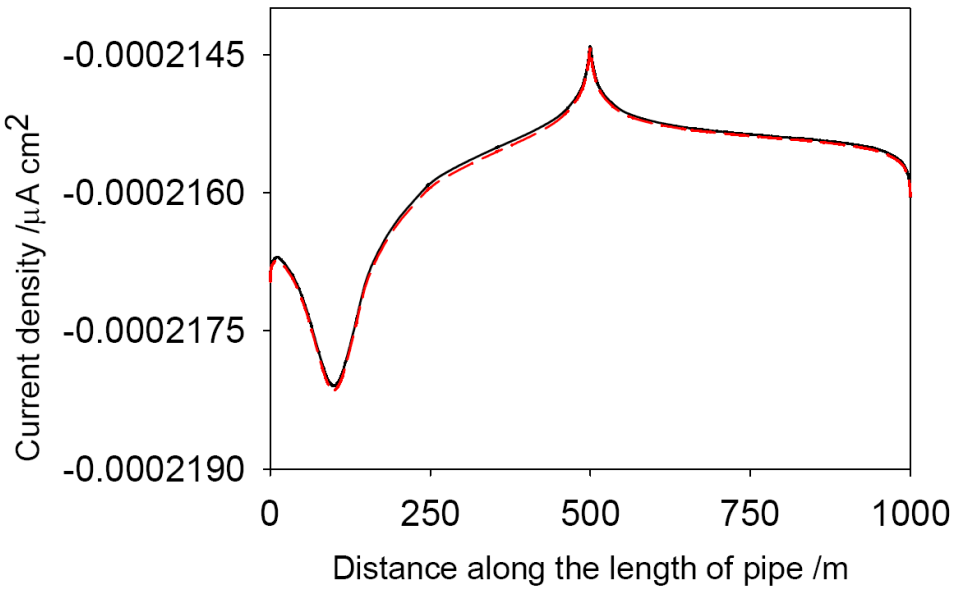

Figure 4-45. Comparison of current density distributions along pipe 1 and pipe 2 respectively in condition 1. Black solid line: pipe 1; red dash line: pipe 2

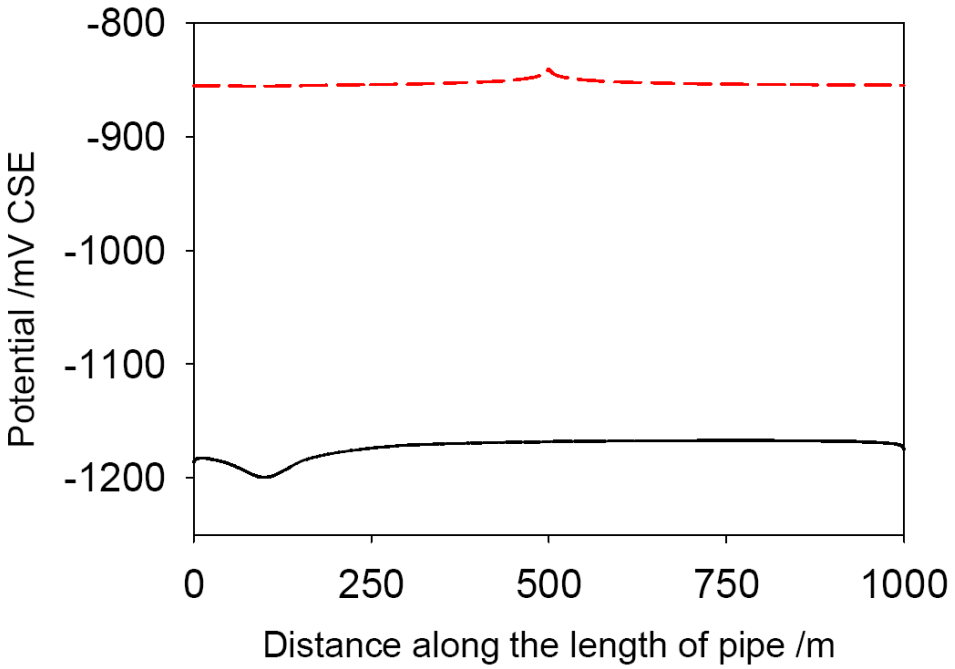

Figure 4-46. Comparison of potential distributions along pipe 1 and pipe 2 respectively in condition 2. Black solid line: pipe 1; red dash line: pipe 2

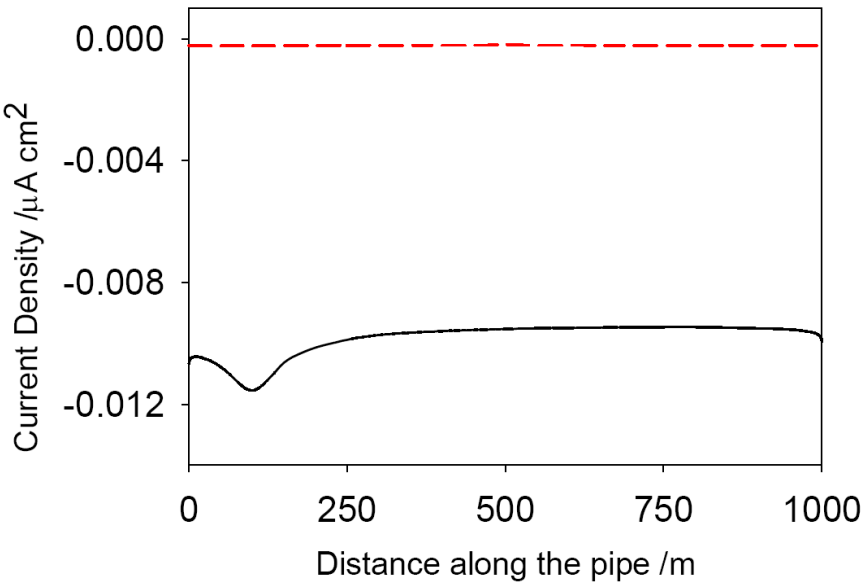

Figure 4-47. Comparison of current density distributions along pipe 1 and pipe 2 respectively in condition 1. Black solid line: pipe 1; red dash line: pipe 2

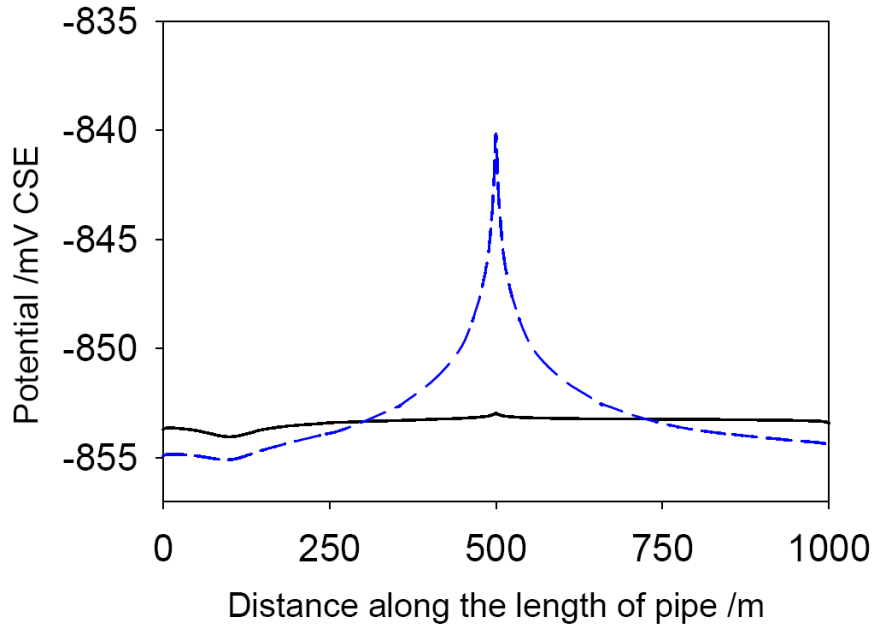

Figure 4-48. Potential distributions of pipe 2 in condition1and 2 respectively. Black solid line: pipe 2 in condition 1; blue dash line: pipe 2 in condition 2

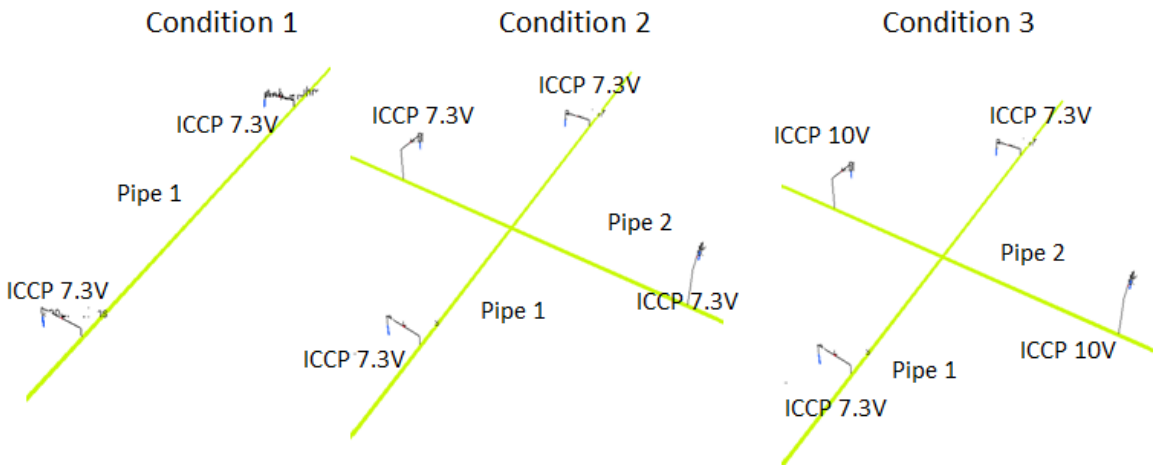

Figure 4-49. Visual configurations of condition 1, 2 and 3 for rectifier war modeling in seawater environment

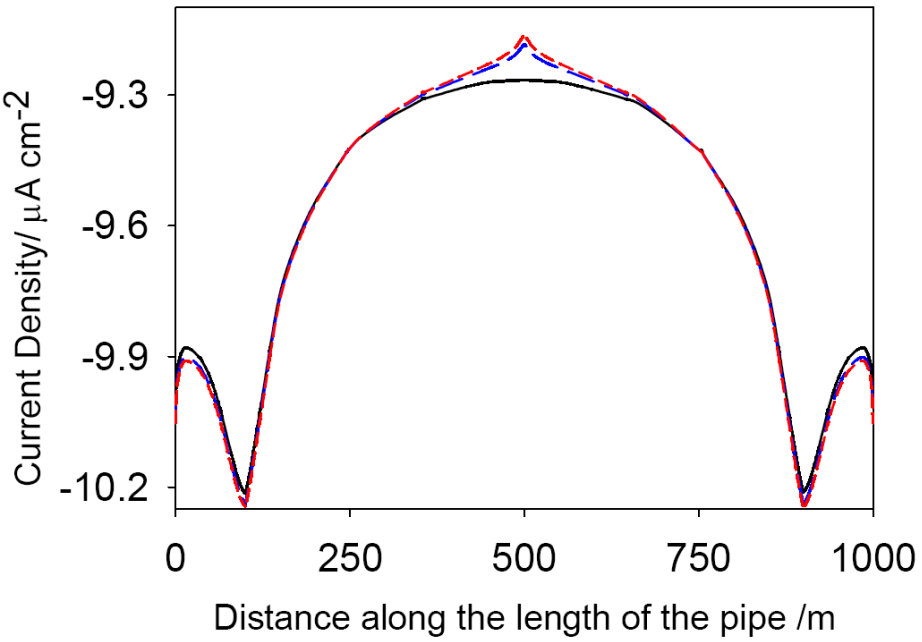

Figure 4-50. Current density distributions of pipe 1 in condition 1, 2 and 3. Black solid line: pipe 1 in condition 1; blue long dash line: pipe 1 in condition 2; red short dash line: pipe 1 in condition 3.

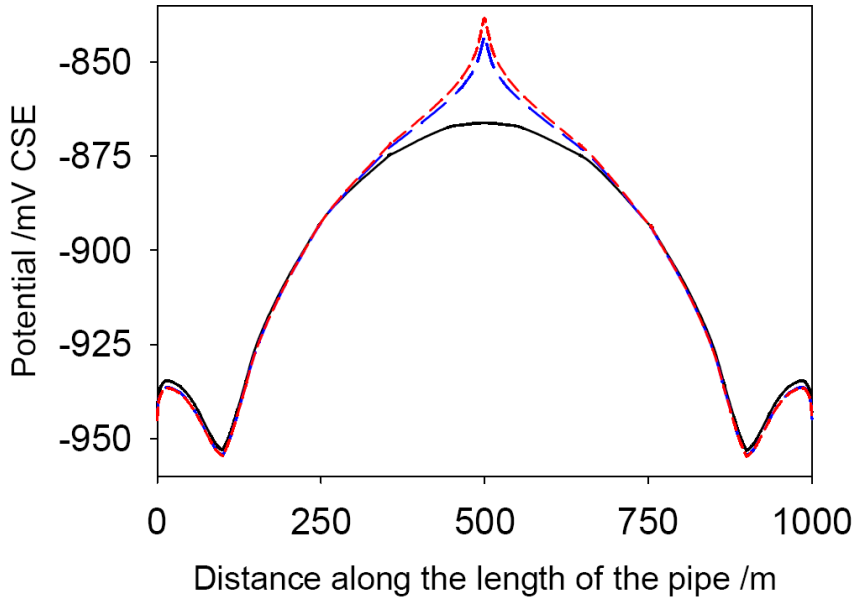

Figure 4-51. Potential distributions of pipe 1 in condition 1, 2 and 3. Black solid line: pipe 1 in condition 1; blue long dash line: pipe 1 in condition 2; red short dash line: pipe 1 in condition 3.

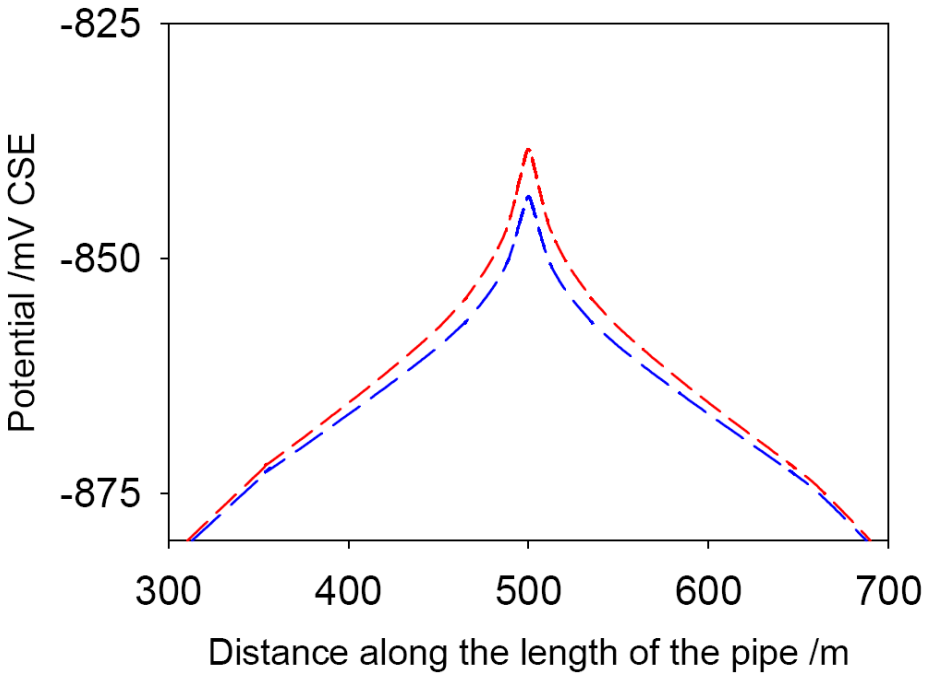

Figure 4-52. A close-up of potential distributions along pipe 1 in condition 2 and 3. Blue long dash line: pipe 1 in condition 2; red short dash line: pipe 1 in condition 3

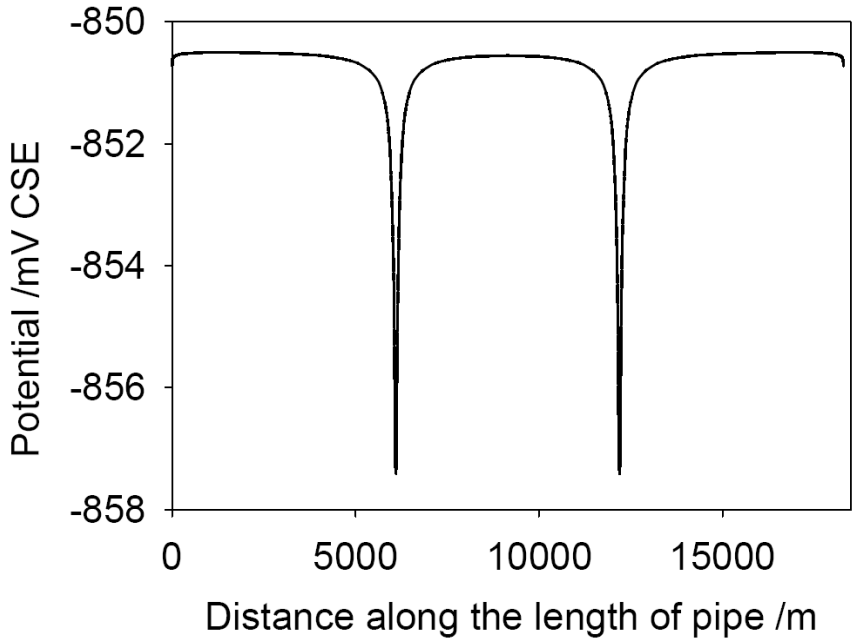

Figure 4-53. Potential distribution along the pipe of 18,300m with two anodes connected.

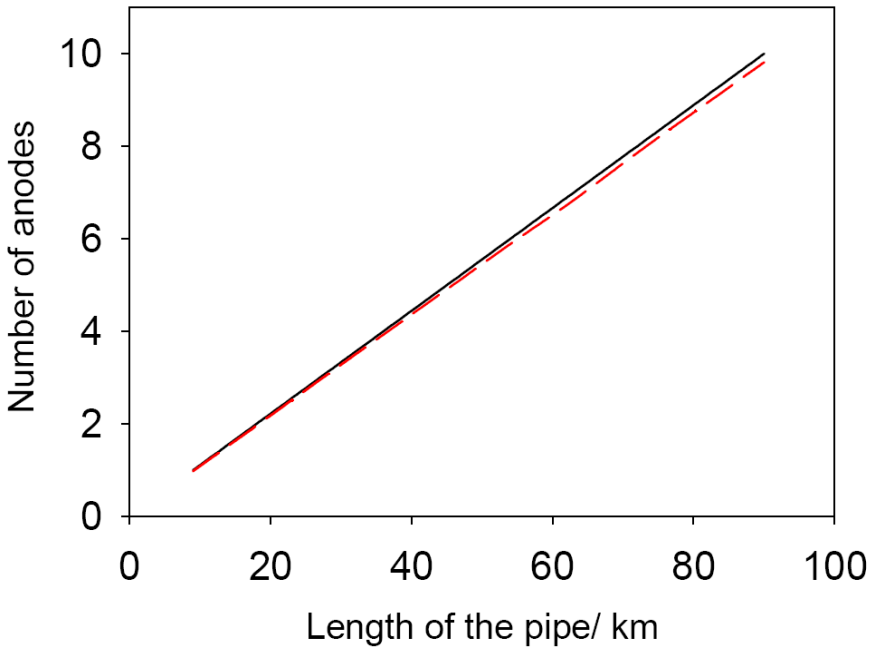

Figure 4-54. Comparison of minimum number of anodes by using CP3D and Dwight Formula in soil environment respectively. Black solid line: CP3D; red dash line: Dwight formula.

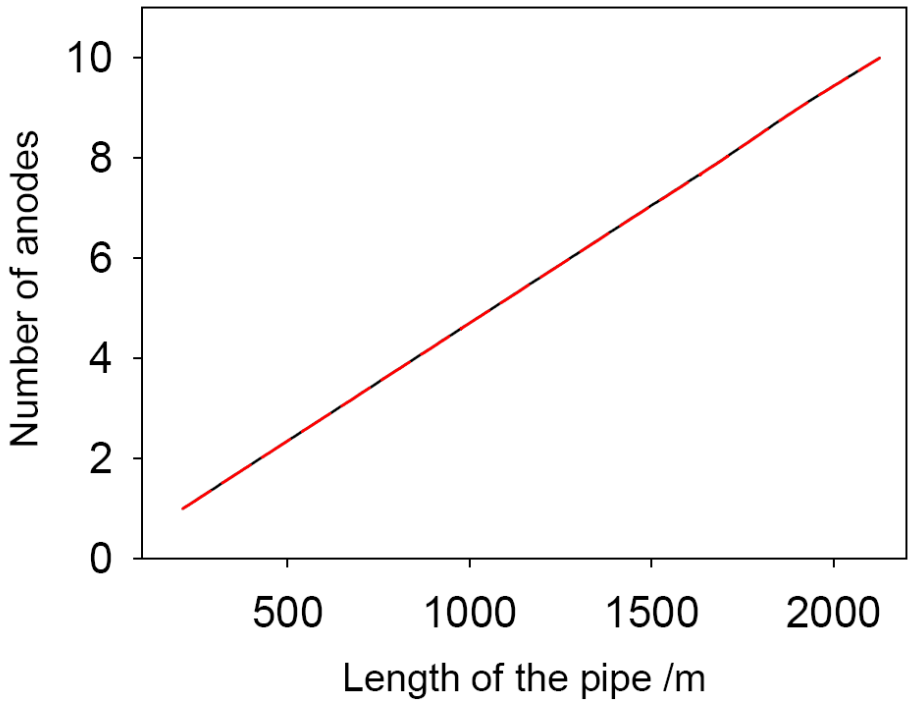

Figure 4-55. Comparison of minimum number of anodes by using CP3D and Dwight Formula in seawater environment respectively. Black solid line: CP3D; red dash line: Dwight formula.

CHAPTER 5
CONCLUSIONS AND FUTURE WORK

Motivated by the Buckingham method, a systematic study of anode parameters was obtained. There are mainly four anode parameters affecting the current density distribution along a single pipe: L_a, D_a, H_a, and, d. Of these, L_a and D_a have larger effect than do H_a and d. This study provides a guideline of choosing proper value of anode parameters to achieve adequate cathodic protection or simulate corrosion behavior in the cathodic protection system.

By choosing proper value of anode variables for the base conditions, stray current effects due to a single anode and due to an anode bed were simulated by applying CP3D. From these simulations, the locations are predicted for sites where localized corrosion is experienced on the unprotected pipes. In addition, stray current modeling methods were applied to rectifier wars. From rectifier war simulations, it is vividly illustrated that a potential difference between cathodic protection systems for two pipes will result in localized corrosion on the pipe with lesser cathodic protection. Hence corresponding measures can be obtained to prevent localized corrosion.

Determination of the minimum number of anodes is a key part of cathodic protection. From this work, two types of minimum current density were obtained in two specific situations: soil environment (off-shore environment) and seawater environment (on-shore environment). The minimum current density needed to protect the pipe with Coating C under the base condition specified is $1.743\times10^{-6}\,\mathrm{A/m^2}$, and minimum current density to protect with Coating A under the base condition specified is $0.08\ \mathrm{A/m^2}$. This

work provides a guideline to determine the minimum number of anodes needed to achieve adequate cathodic protection.

For the future work, the first suggestion is to develop a similar dimensional analysis in secondary current distribution condition in which kinetics resistance is considered. The second suggestion is to determine the length of the section along the unprotected pipe which experiences localized corrosion quantitatively. The last suggestion is to simulate alternating stray current corrosion and develop an effective mathematical model to predict the potential and current distribution in this situation.

LIST OF REFERENCES

[1] G.H. Koch, M.P. H Brongers, N.G. Thompson, Y.P. Virmani, J.H. Payer, Corrosion costs and preventive strategies in the Unites States, NACE International, Houston, Texas, 2001.

[2] NTSB, Pipeline Accident Report: Pipeline Rupture and Release of Fuel Oil into the Reedy River, Fork Shoals, South Carolina June 26 1996, Technical report, National Transportation Safety Board, Washington, D.C. 1998.

[3] M.G. Fontana, Corrosion Engineering, 3rd ed., McGraw-Hill, Singapore, 1986.

[4] A.J. Bard, L.R. Faulkner, Electrochemical Methods: Fundamentals and Applications, Wiley, New York, 1980.

[5] J.O. Bockris, D. Drazic, A.R. Despic, The Electrode kinetics of the deposition and dissolution of iron, Electrochimica Acta 4 (1961) 325–361.

[6] J. Wagner, Cathodic Protection Design I, NACE International, Houston, Texas, 1994.

[7] G. Jerkiewicz, Hydrogen sorption at/In electrode, Progress in Surface Science 57 (1998) 137–186.

[8] M. de Chialvo, A. Chialvo, The Tafel-Heyrovsky route in the kinetic mechanism of the hydrogen evolution reaction, Electrochemistry Communications 1 (1999) 379–382.

[9] M. de Chialvo, A. Chialvo, Existence of two sets of kinetic parameters in the correlation of the hydrogen electrode reaction, Journal of the Electrochemical Society 147 (2000) 1619–1622

[10] A. Lasia, D. Gregoire, General model of electrochemical hydrogen absorption into metals, Journal of the Electrochemical Society 142 (1995) 3393–3399.

[11] L.J. Bai, Behavior of a hydride phase formed in the hydrogen evolution reaction at a rotating Pt electrode - analysis of potential relaxation transients from a kinetic approach, Journal of Electroanalytical Chemistry 355 (1993) 37–55.

[12] D.P. Riemer, Modeling cathodic protection for pipeline networks, Ph.D. dissertation, the University of Florida, Gainesville, Florida, 2000.

[13] K. Nisancioglu, Predicting the time dependence of polarization on cathodically protected steel in seawater, Corrosion 43 (1987) 100–111.

[14] K. Nisancioglu, P.O. Gartland, T. Dahl, E. Sander, Role of surface structure and flow rate on the polarization of cathodically protected steel in seawater, Corrosion 43 (1987) 710–718.

[15] K. Nisancioglu, P.O. Gartland, Current distribution with dynamic boundary conditions, in: Conference on Electrochemical Engineering, vol. 112 of I.Chem. Symposium Series, Loughborough University of Technology, Loughborough, 1989.

[16] J.F. Yan, S.N.R. Pakalapati, T.V. Nguyen, R.E. White, R.B. Griffin, Mathematical modeling of cathodic protection using the boundary element method with a nonlinear polarization curve, Journal of the Electrochemical Society 139 (1992) 1932–1936.

[17] K. Kennelley, L. Bone, M. Orazem, Current and potential distribution on a coated pipeline with holidays Part I - model and experimental verification. Corrosion 49 (1993) 199–210.

[18] J. Morgan, Cathodic Protection, 2nd ed., NACE International, Houston, Texas, 1993.

[19] D. Riemer, M. Orazem, Development of mathematical models for cathodic protection of multiple pipelines in a right of way, Proceedings of the 1998 International Gas Research Conference 117 (1998) 19.

[20] D. Riemer, M. Orazem, Cathodic protection of multiple pipelines with coating holidays, Procedings of the NACE1999 Topical Research Symposium (1999) 65–81.

[21] J.S. Newman, Electrochemical Engineering, 2nd ed., Prentice-Hall, Englewood Cliffs, New Jersey:, 1991.

[22] C.A. Brebbia, J. Dominguez, Boundary element methods for potential problems, Applied Mathematical Modeling 1 (1977) 371–378.

[23] S. Aoki, K. Kishimoto, M. Sakata, Boundary element analysis of galvanic corrosion, Boundary Elements VII 1 (1985) 73–83.

[24] S. Aoki, K. Amaya, Optimization of cathodic protection system by BEM, Engineering Analysis with Boundary Elements 19 (1997) 147–156.

[25] F. Brichau, J. Deconinck, Numerical model for cathodic protection of buried pipes, Corrosion 50 (1994) 39–49.

[26] F. Hartmann, C. Katz, B. Protopsaltis, Boundary elements and symmetry, INGENIEUR ARCHIV 55 (1985) 440–449.

[27] C.J Geankoplis, Transport Processes and Unit Operations, 3rd ed.,Prentice Hall, Englewood Cliff, New Jersey, 1993.

BIOGRAPHICAL SKETCH

Chao Liu graduated from Nanchang University in China, with a Bachelor of Science degree in applied chemistry in July 2010. He enrolled in the Master of Engineering program in chemical engineering at the University of Florida in August 2010. Then he transferred to the Master of Science program and joined Professor Mark E. Orazem's research group, working on the project of CP3D simulation on buried pipeline corrosion. He received his Master of Science degree from the University of Florida in May 2012.